Supporting information

Magnetically separable core/shell Iron oxide@Nickel nanoparticles as high-performance recyclable catalysts for chemoselective reduction of nitroaromatics

Puran Singh Rathore[a], Rajesh Patidar[b], T. Shripathi[c], Sonal Thakore[a]*

[a]Department of Chemistry, Faculty of Science,

The M. S. University of Baroda, Vadodara, 390002, India

[b]Analytical Discipline and CIF, Central Salt and Marine Chemicals Research Institute (CSIR-CSMCRI), G. B. Marg, Bhavnagar, 364002, Gujarat, India

[c]UGC-DAE Consortium for Scientific Research, Indore 452 001, India

Primary constitutes of the IOTs selected for the present study are Fe, Si and Al (Fe_2O_3, 53.68; SiO_2, 17.58; Al_2O_3, 14.46; P_2O_5, 1.61; CaO, 1.44, MgO, 0.13; LOI, 10.01 wt %).

Fig.S1 XRD pattern shows that Maghemite, Magnetite (θ=44.97) and kaolinite (θ=21.18) are present in the IOTs.

Fig.3 shows that, under optimum conditions (Table-1, entry-6) when the quantity of substrate was increased the reaction time decreased. Similarly, when quantity of solvent (water) was decreased the reaction time increased.

The FT-IR spectra of pure starch (Fig.S4A) and IO@NiNPs (Fig.S4B) both display the typical profile of polysaccharides in the range 920–1100 cm^{-1} (characteristic peaks attributed to C-C/C-O bond stretching). The peaks at 1020–1100 cm^{-1} are characteristic of the anhydroglucose ring. The peaks at 1402–1420 cm^{-1} are due to C-H bending. It is seen that the peak at 1642 cm^{-1} shifts

to 1623 cm^{-1} in the IO@NiNPs. The shifts observed in the spectra can be attributed to the interaction of NPs with starch. The band at 2901–2928 cm^{-1} is characteristic of C–H stretching. A broad band due to hydrogen bonded hydroxyl group (O–H) appeared at 3400–3420 cm^{-1} and is attributed to the complex vibrational stretching, associated with free, inter and intra molecular bound hydroxyl groups.

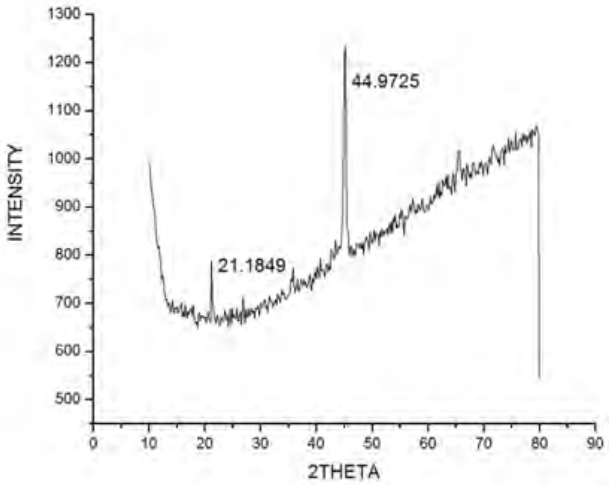

Fig. S1 XRD pattern of IOTs

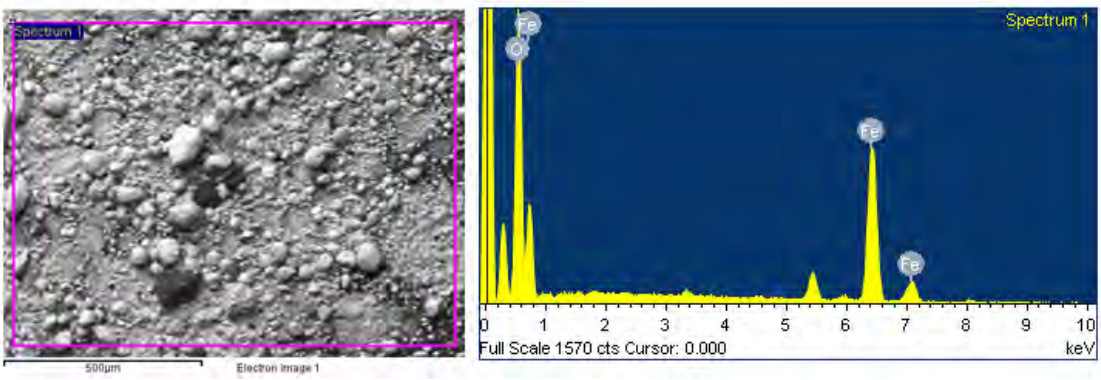

Fig. S2 SEM-EDX analysis of Iron oxide

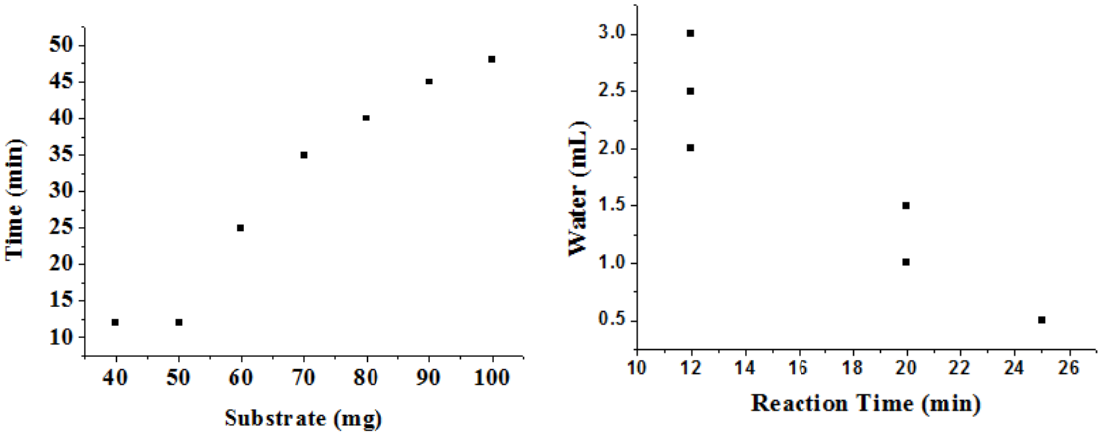

Fig. S3 Reduction of PNA to PPDA at different concentration of substrate and water (under optimum conditions)

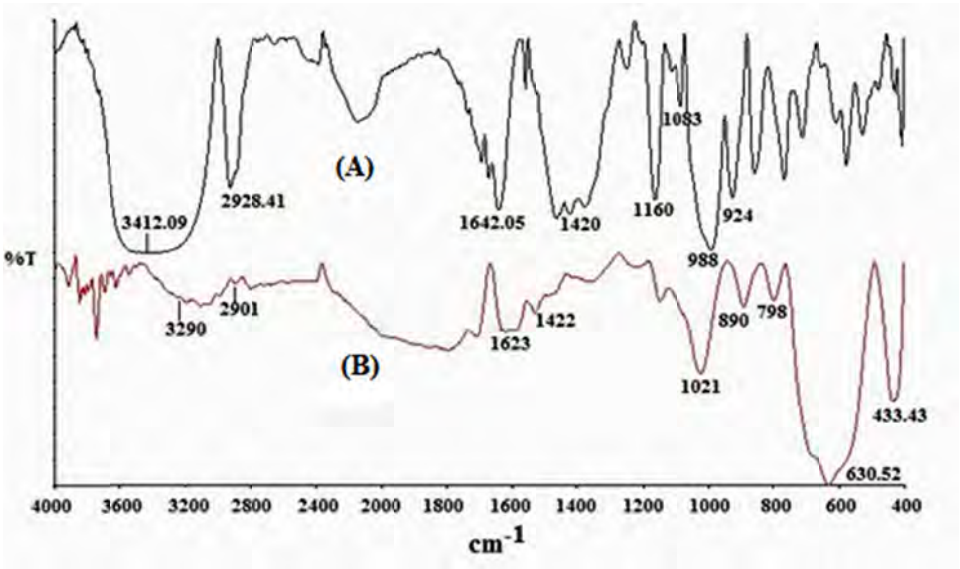

Fig. S4 FT-IR spectra of (A) Starch and (B) Starch capped IO@NiNPs

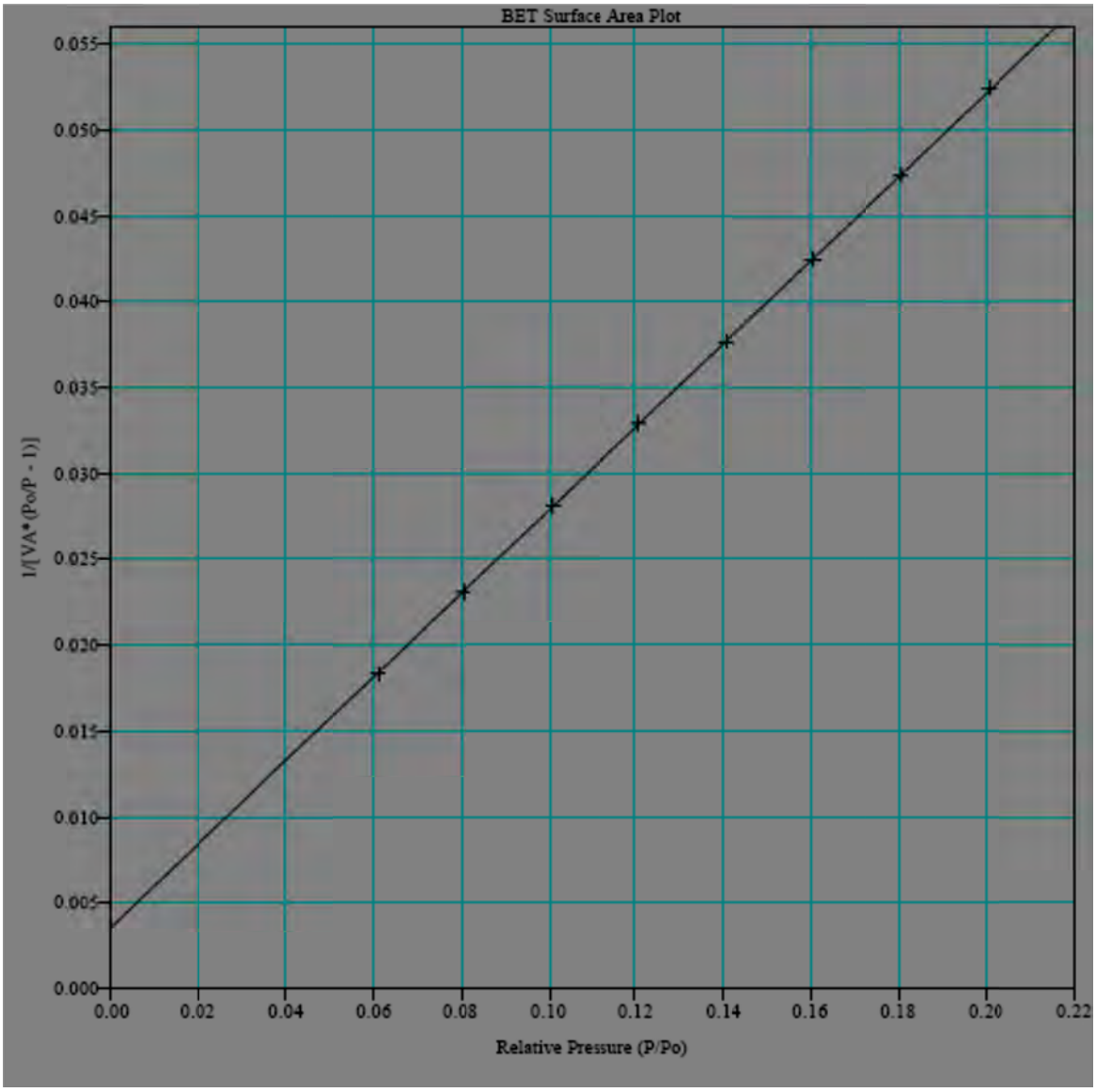

Fig.S5 BET Surface area Plot for IO@NiNPs

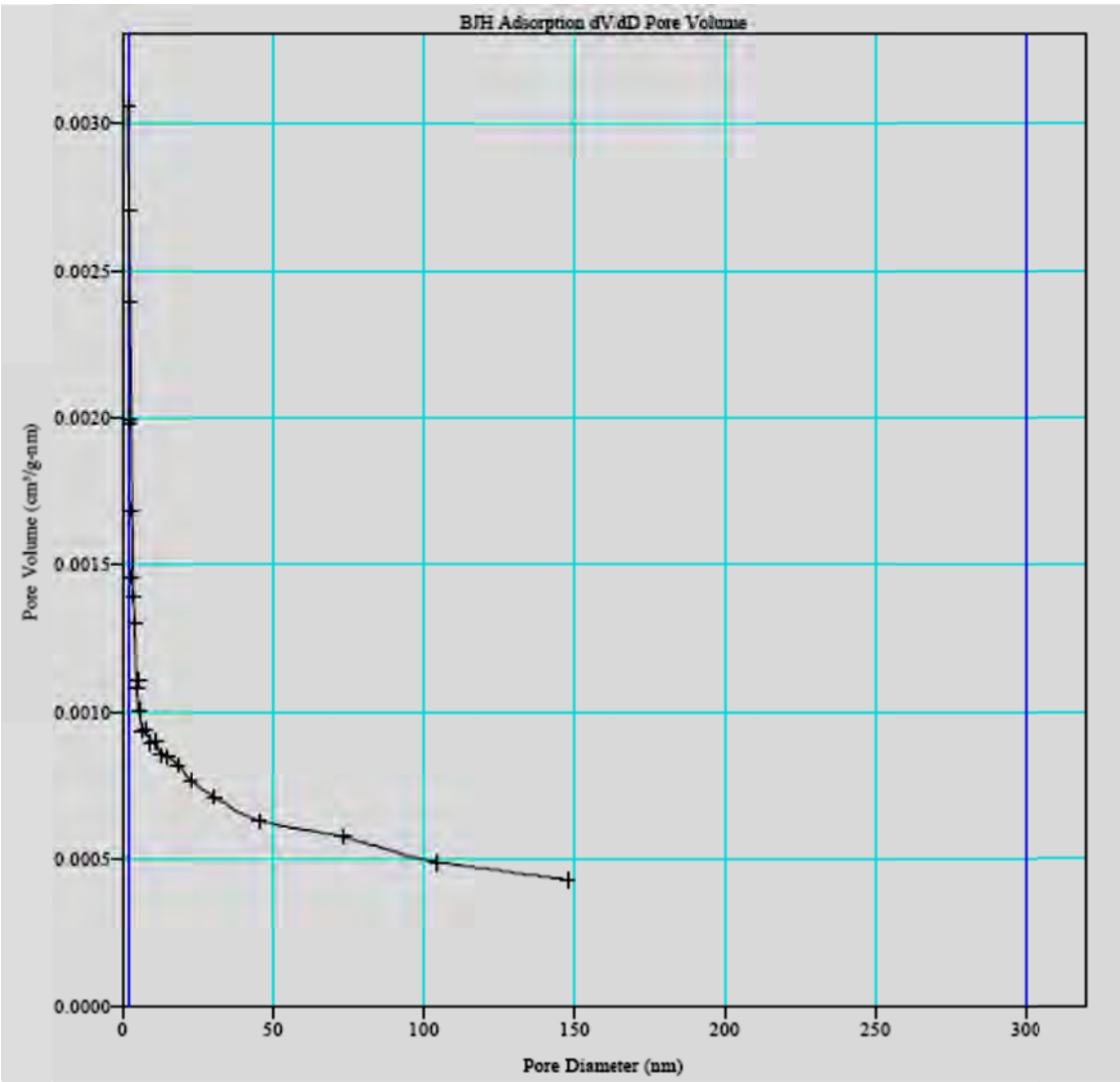

Fig. S6 BJH Adsorption dV/dD Pore Volume for IO@NiNPs

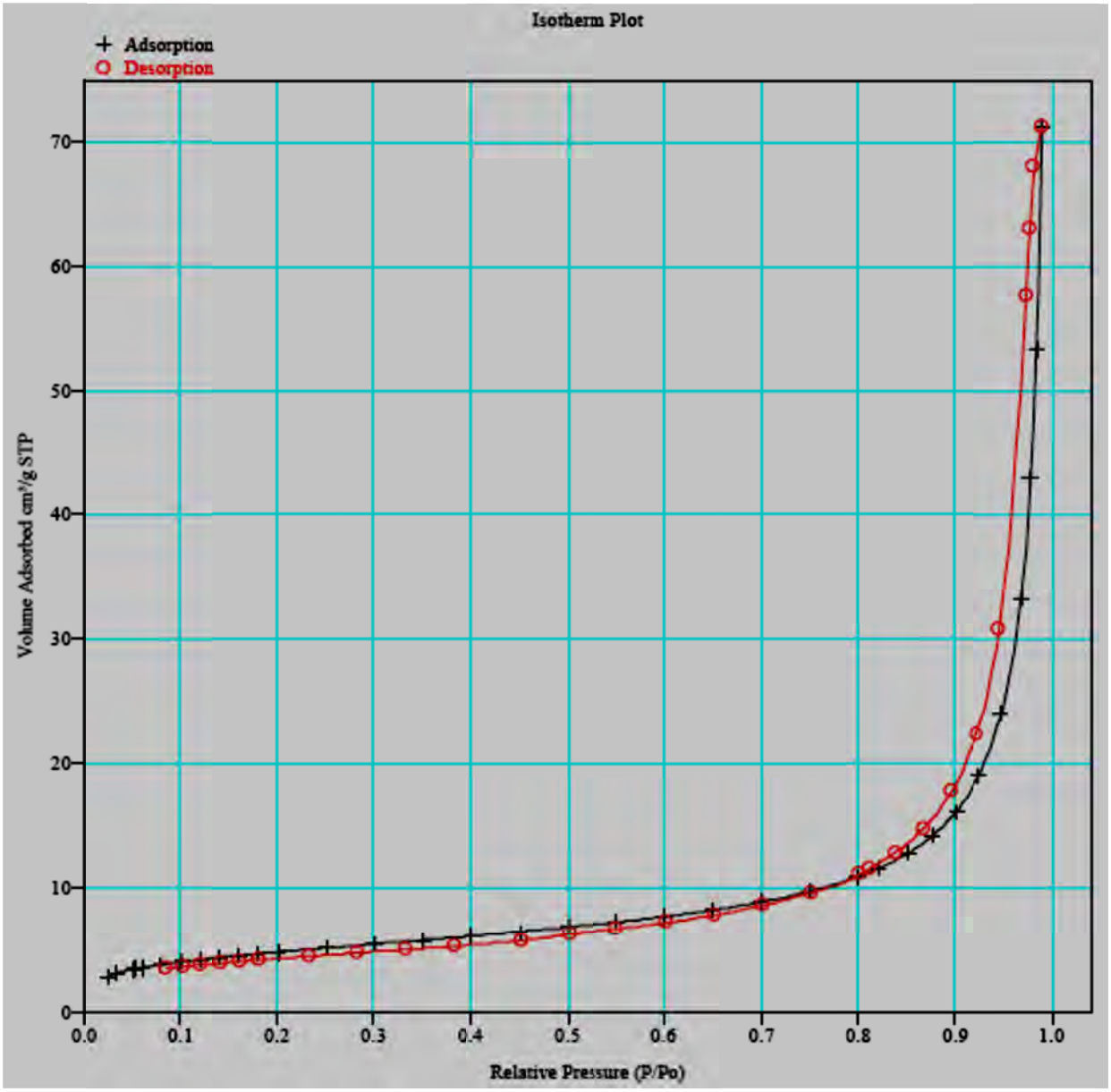

Fig. S7 BET Isotherm Plot for IO@NiNPs

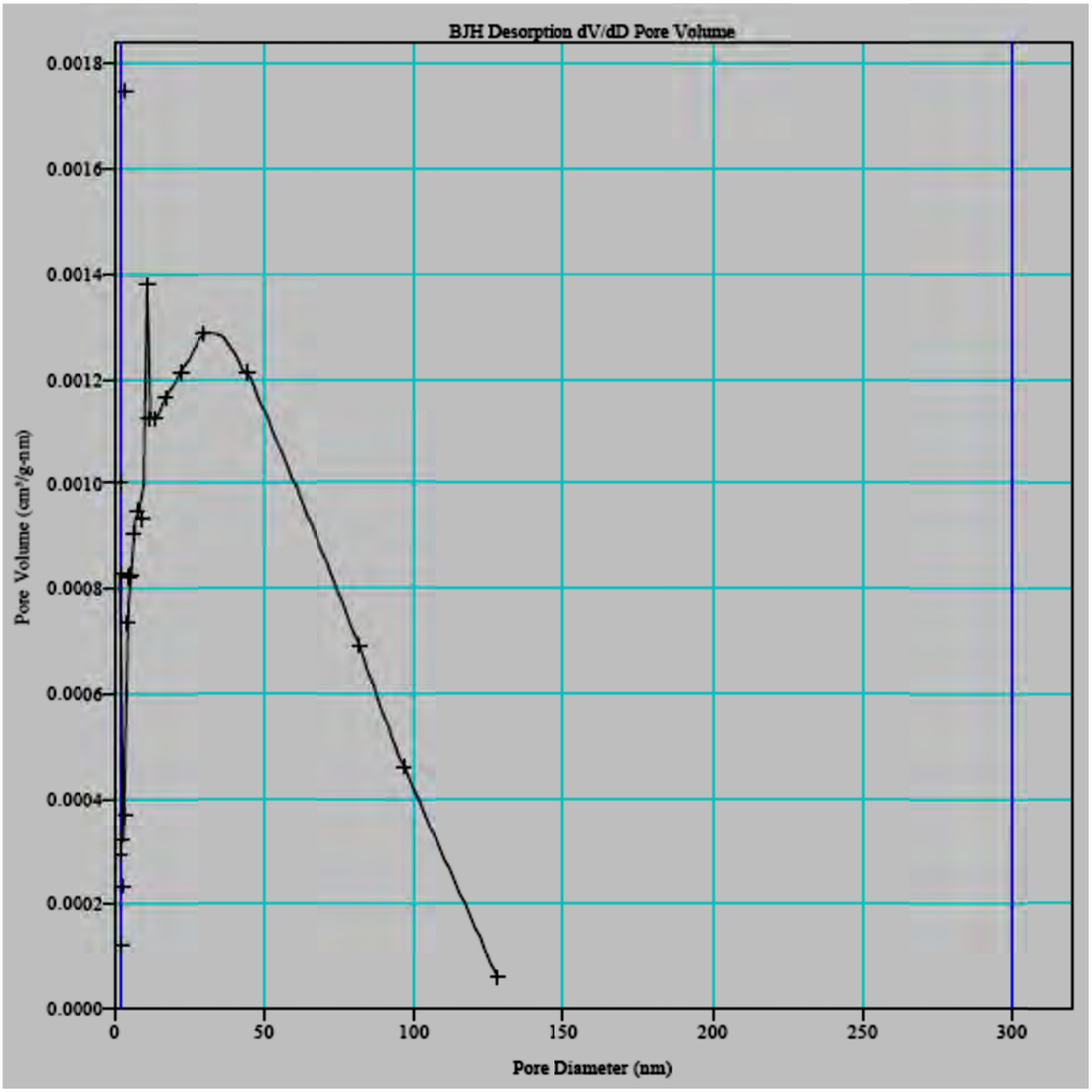

Fig. S8 BJH Desorption dV/dD Pore Volume for IO@NiNPs

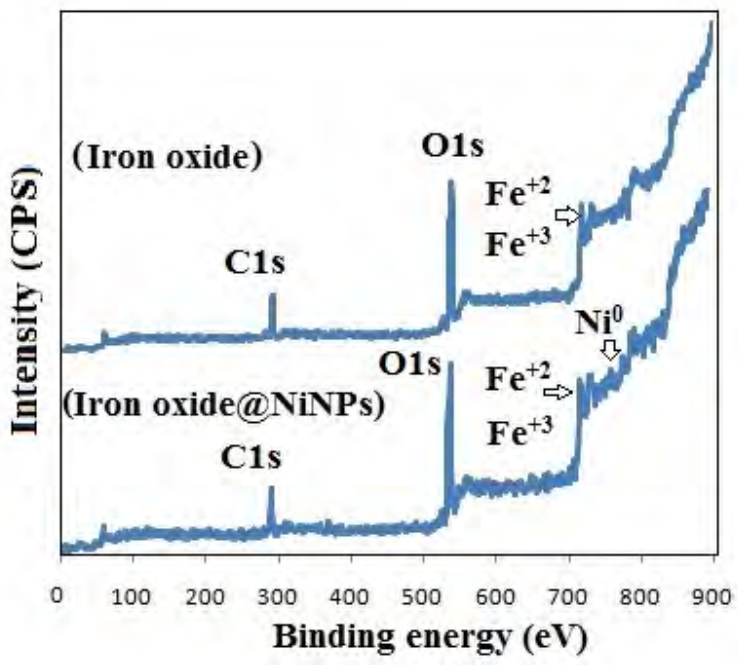

Fig. S9 XPS analysis of Iron oxide and IO@NiNPs

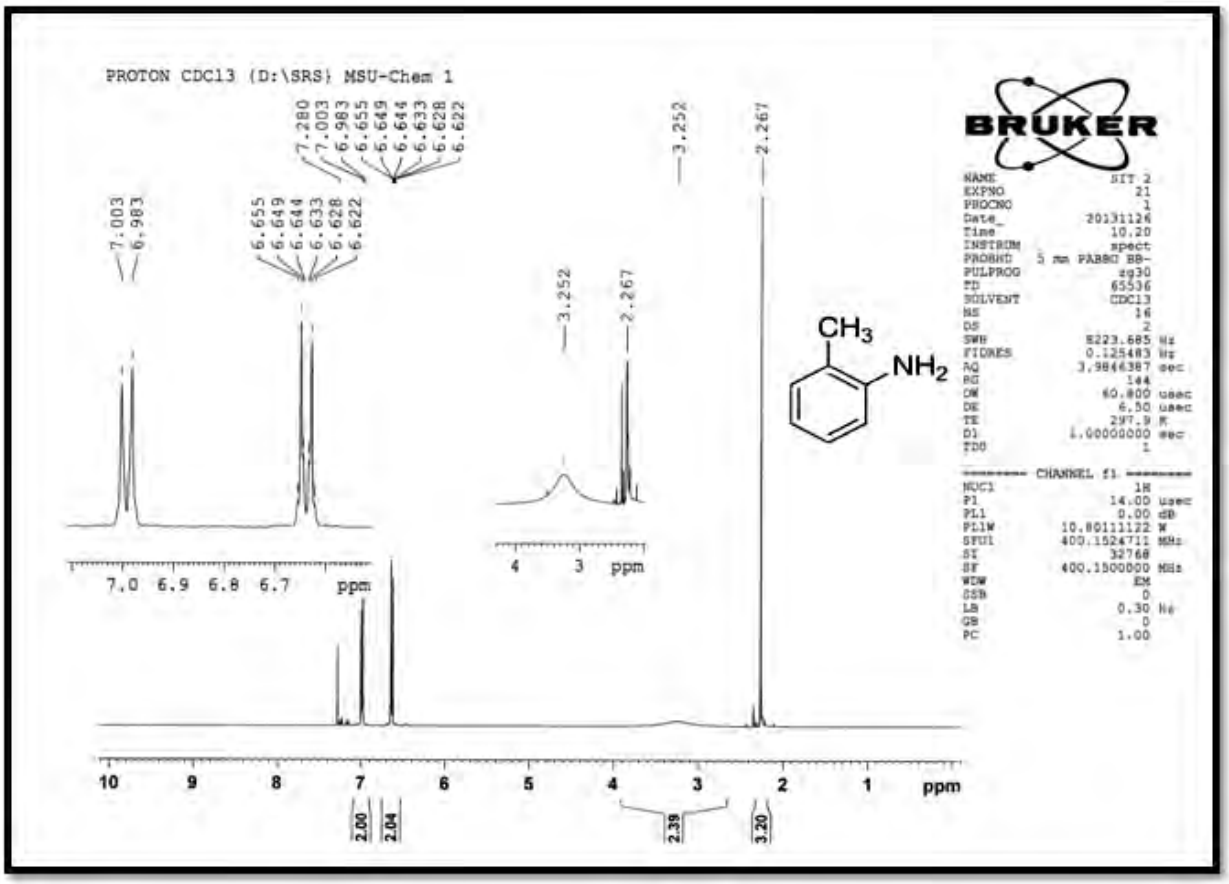

Fig. S10 ^{1}HNMR spectra of *o*-Toulidine ($CDCl_3$, Table-2, Entry-1)

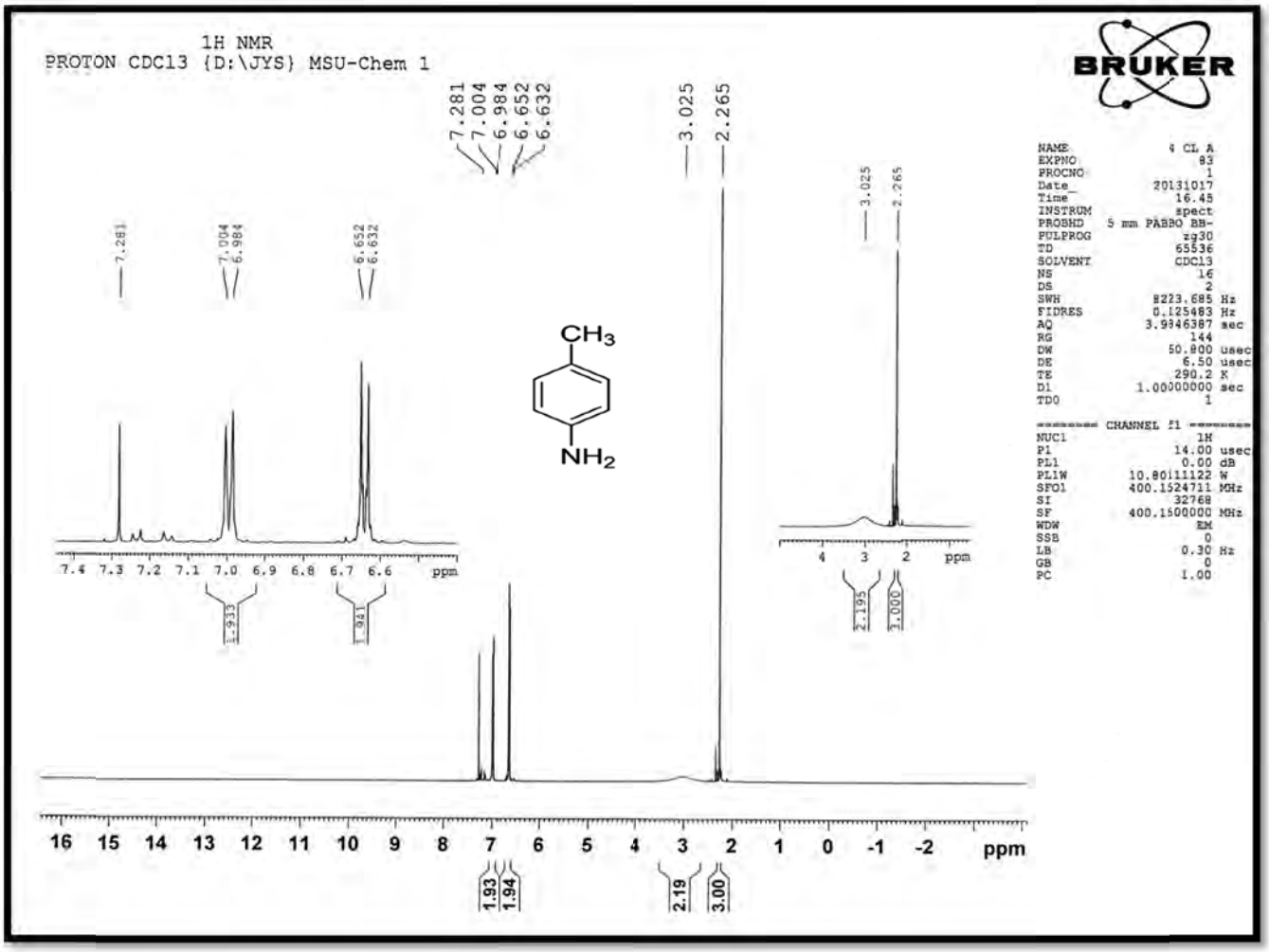

Fig. S11 ^{1}HNMR spectra of *p*-Toulidine ($CDCl_3$, Table-2, Entry-2)

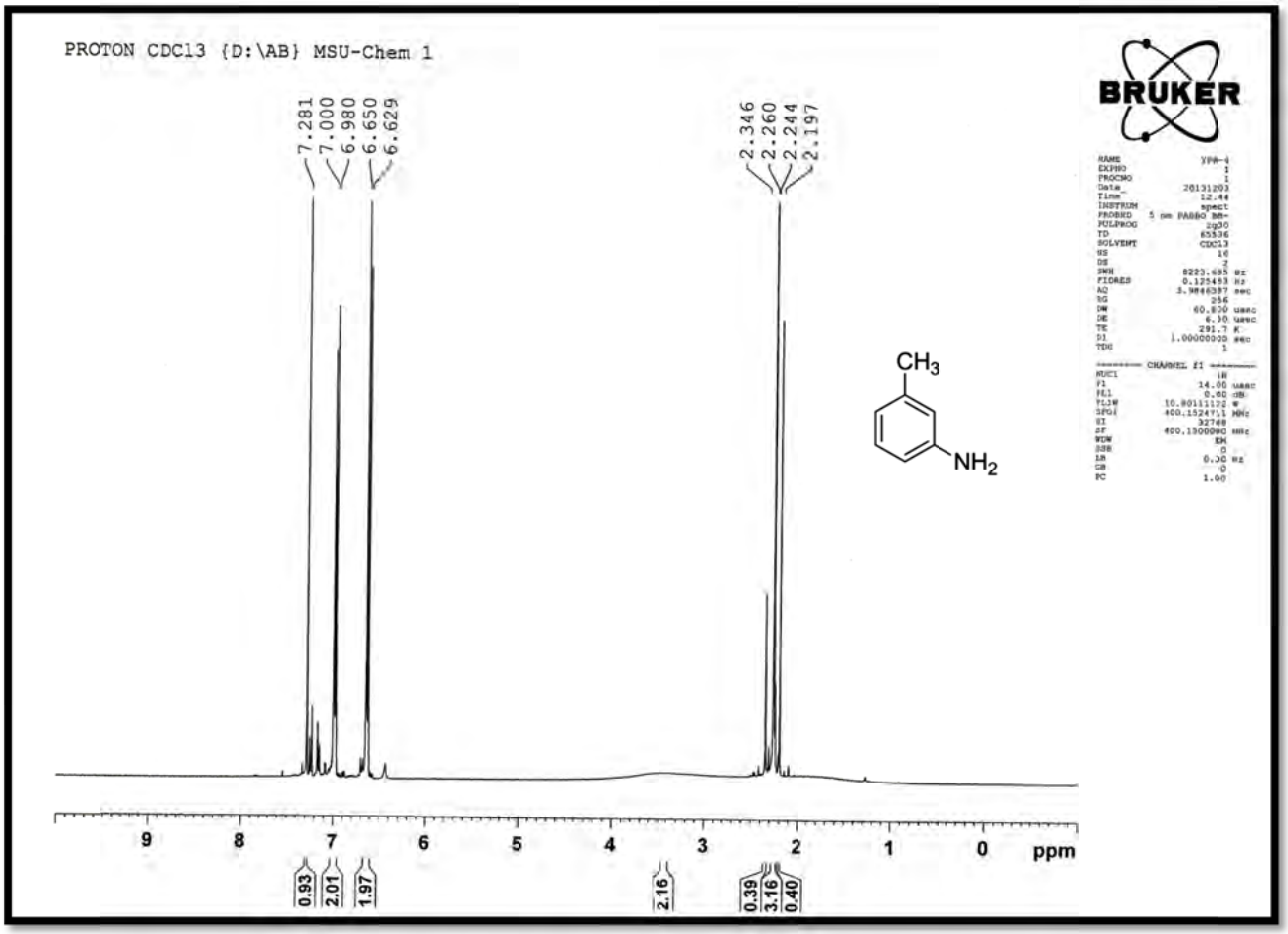

Fig. S12 ^{1}HNMR spectra of *m*-Toulidine ($CDCl_3$, Table-2, Entry-3)

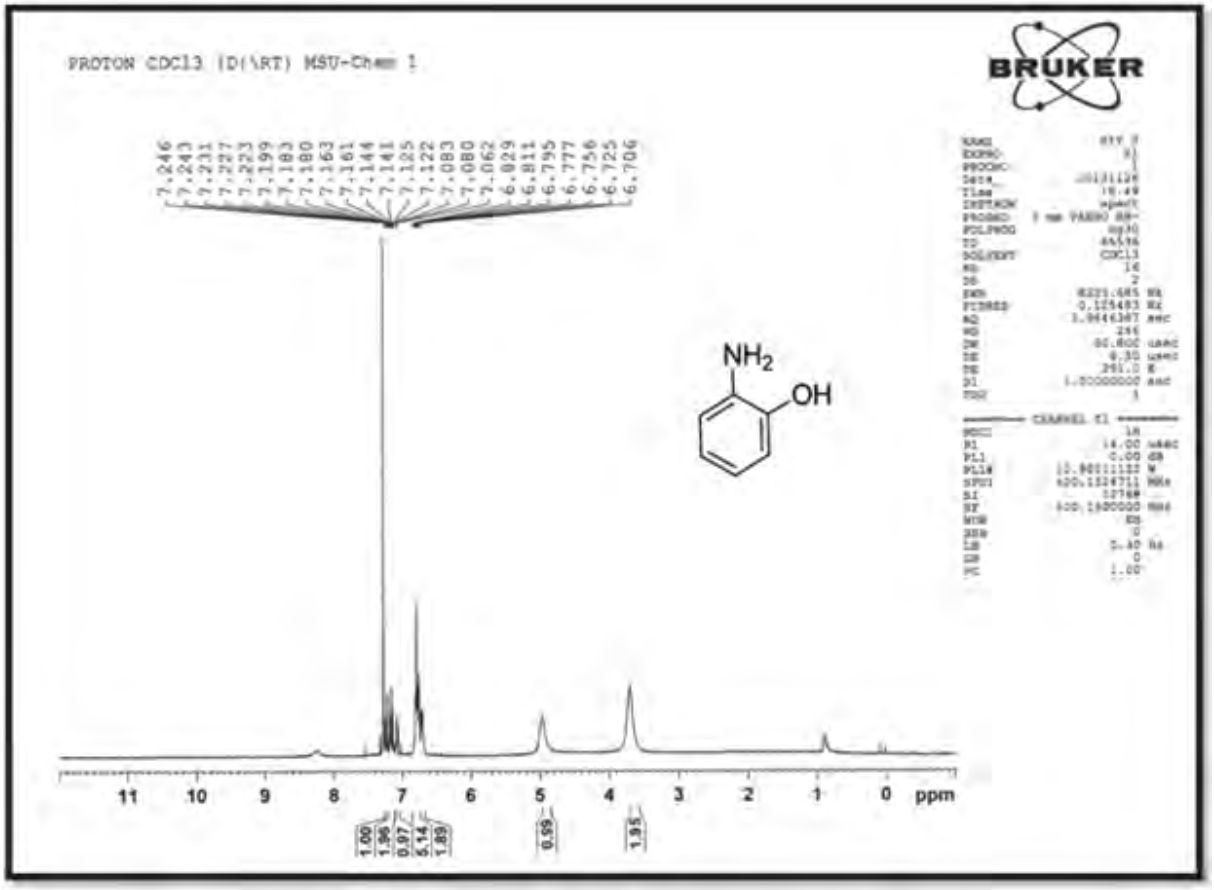

Fig. S13 ^{1}HNMR spectra of *o*-Aminophenol ($CDCl_3$, Table-2, Entry-4)

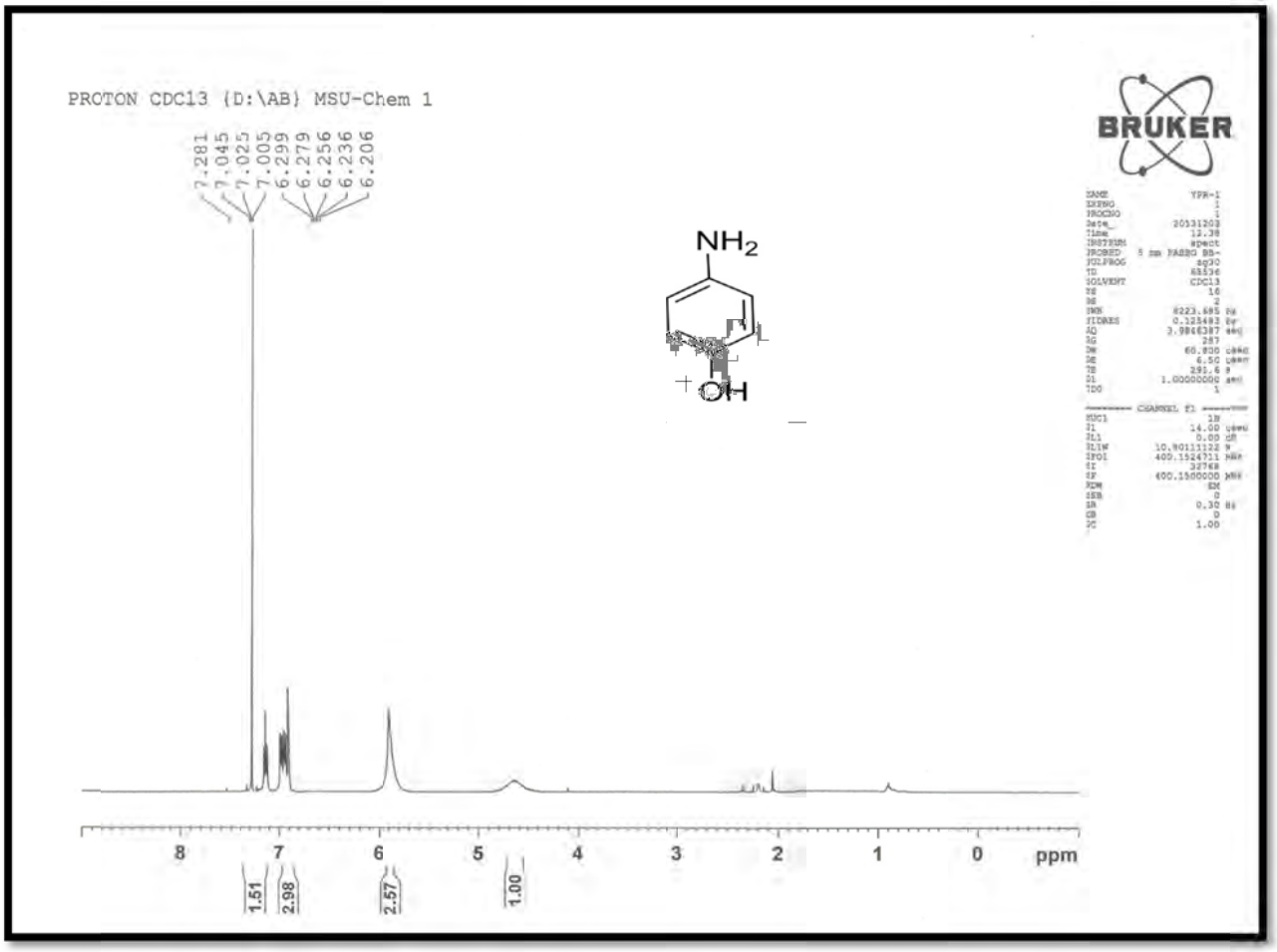

Fig. S14 ^{1}HNMR spectra of *p*-Aminophenol ($CDCl_3$, Table-2, Entry-5)

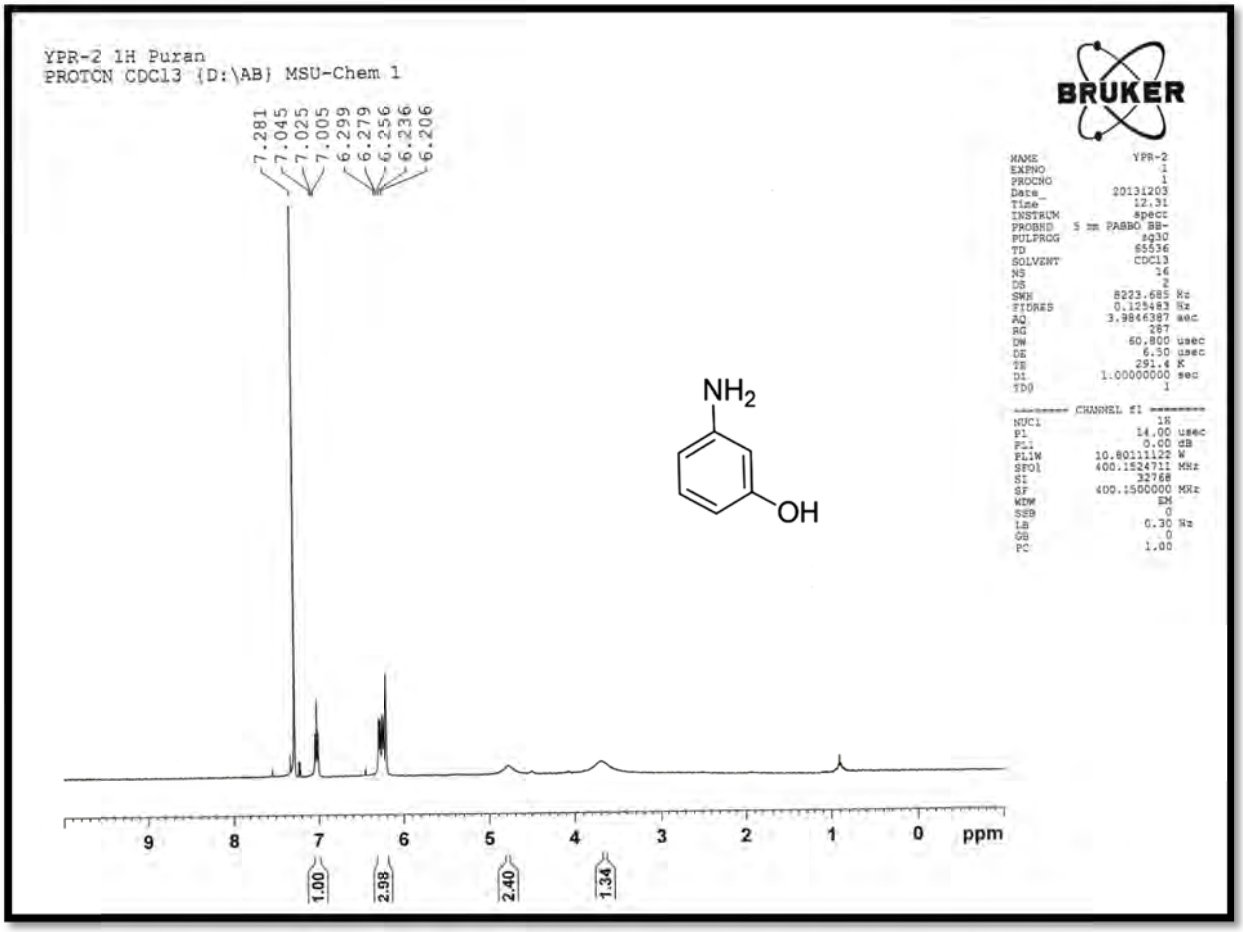

Fig. S15 ^{1}HNMR spectra of *m*-Aminophenol ($CDCl_3$, Table-2, Entry-6)

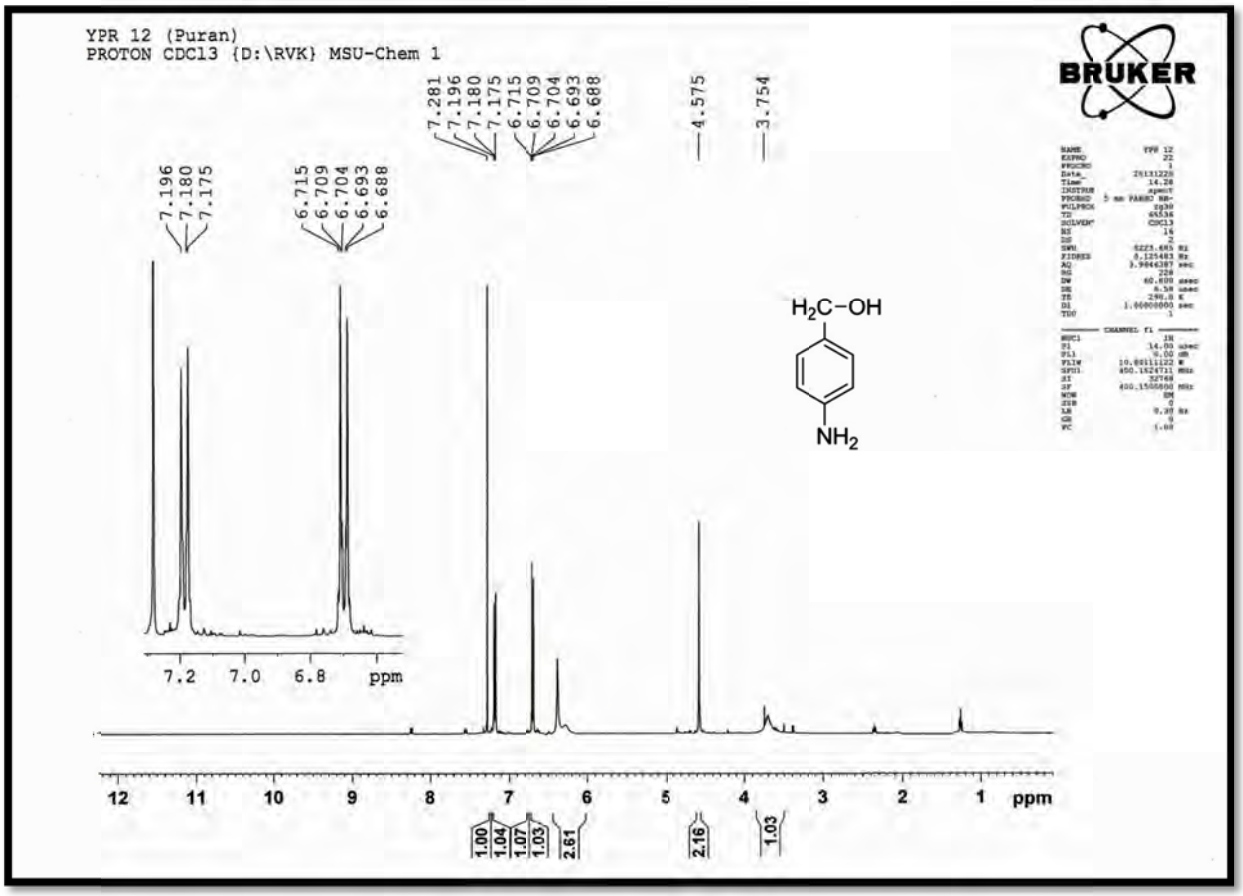

Fig. S16 ^{1}HNMR spectra of *p*-Aminobenzyl alcohol ($CDCl_3$, Table-2, Entry-7)

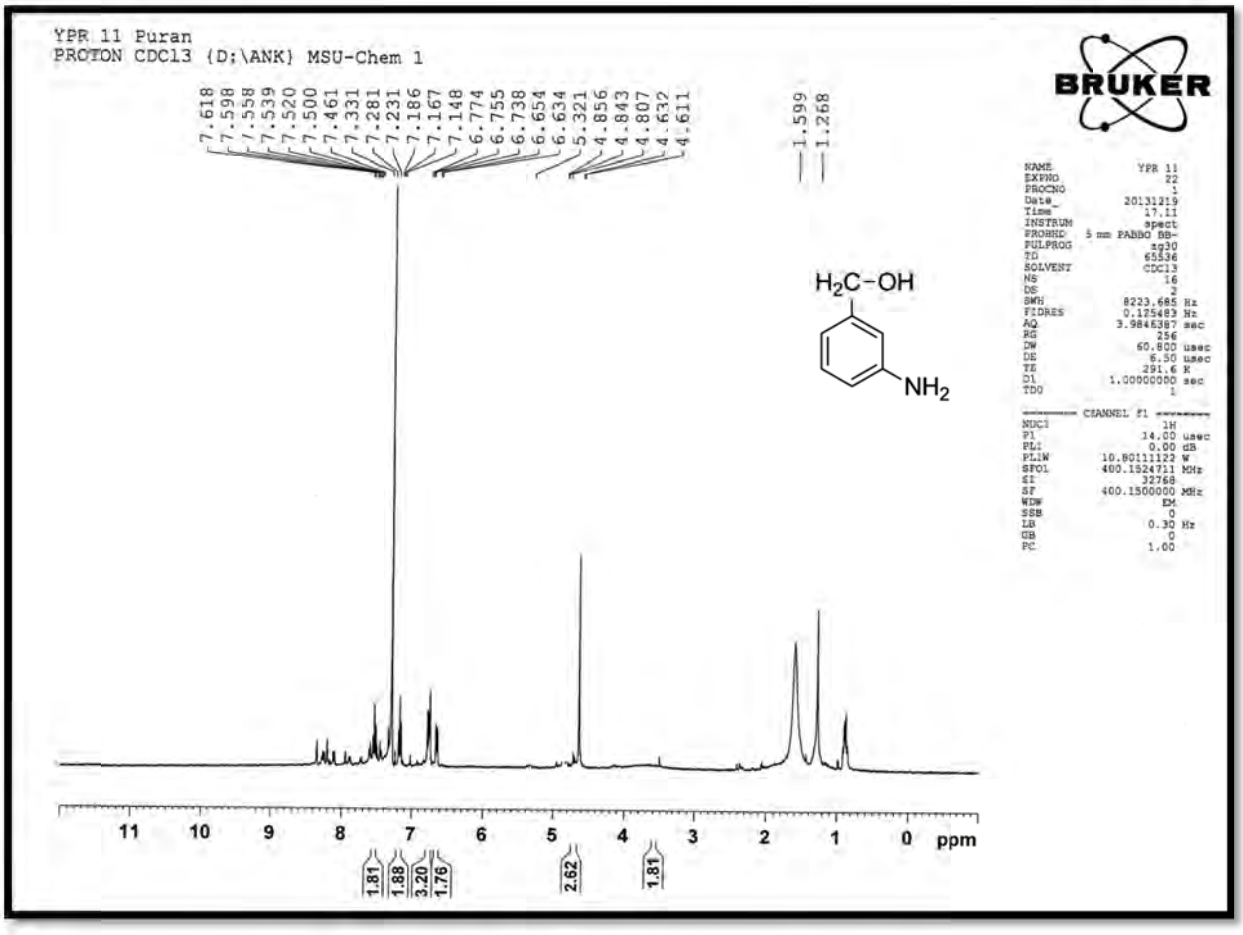

Fig. S17 ^{1}HNMR spectra of *m*-Aminobenzyl alcohol ($CDCl_3$, Table-2, Entry-8)

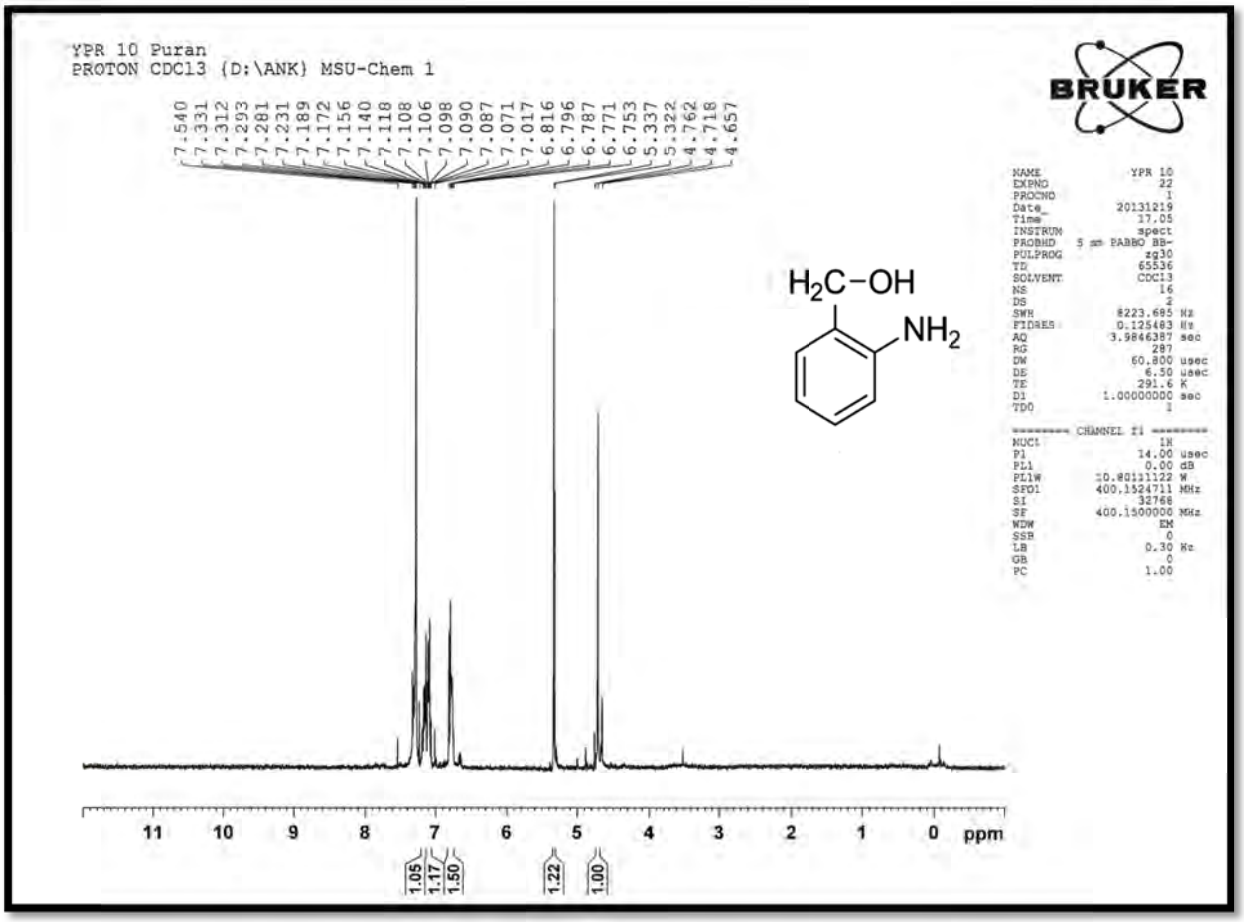

Fig. S18 ^{1}HNMR spectra of *o*-Aminobenzyl alcohol ($CDCl_3$, Table-2, Entry-9)

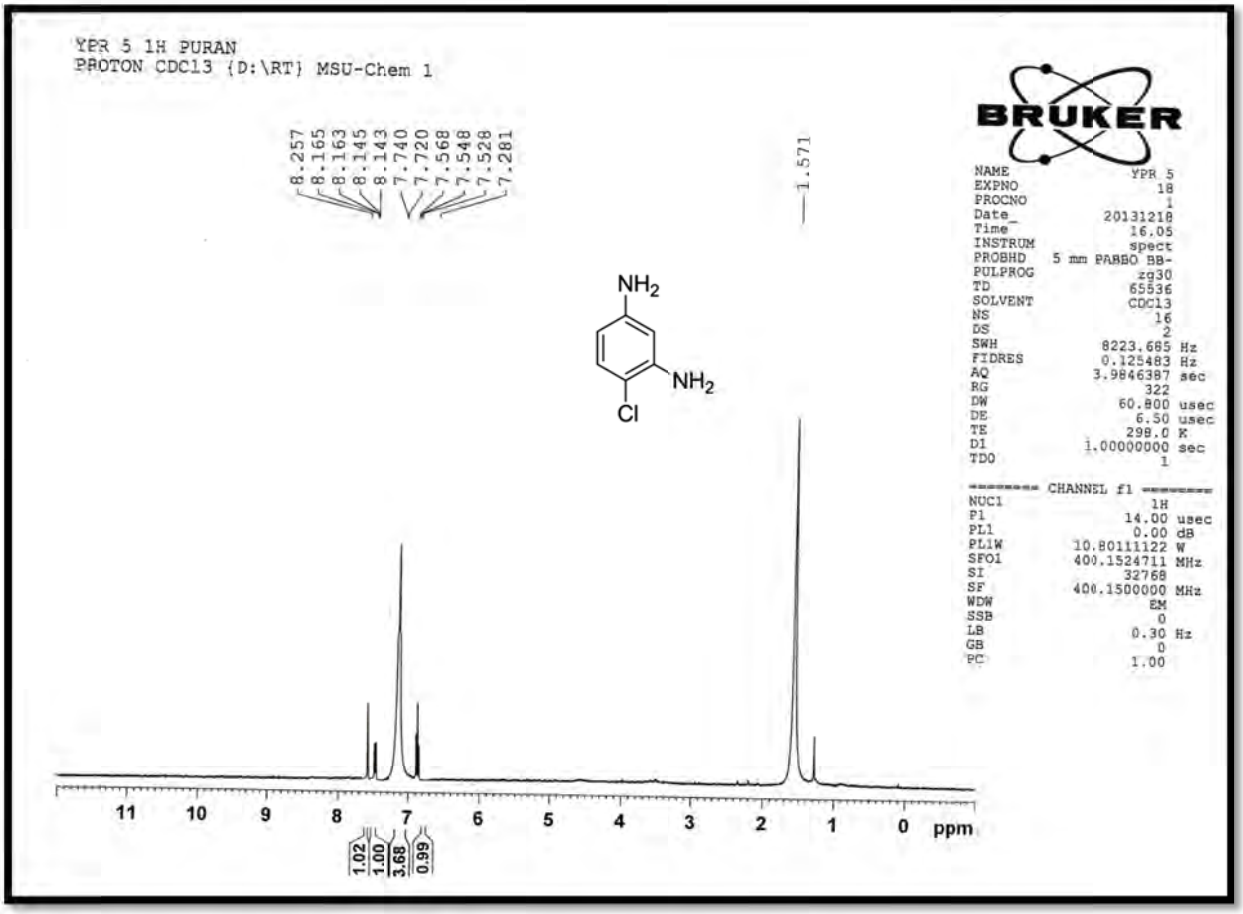

Fig. S19 ^{1}HNMR spectra of 4-Chlorobenzene-1,3-diamine ($CDCl_3$, Table-2, Entry-10)

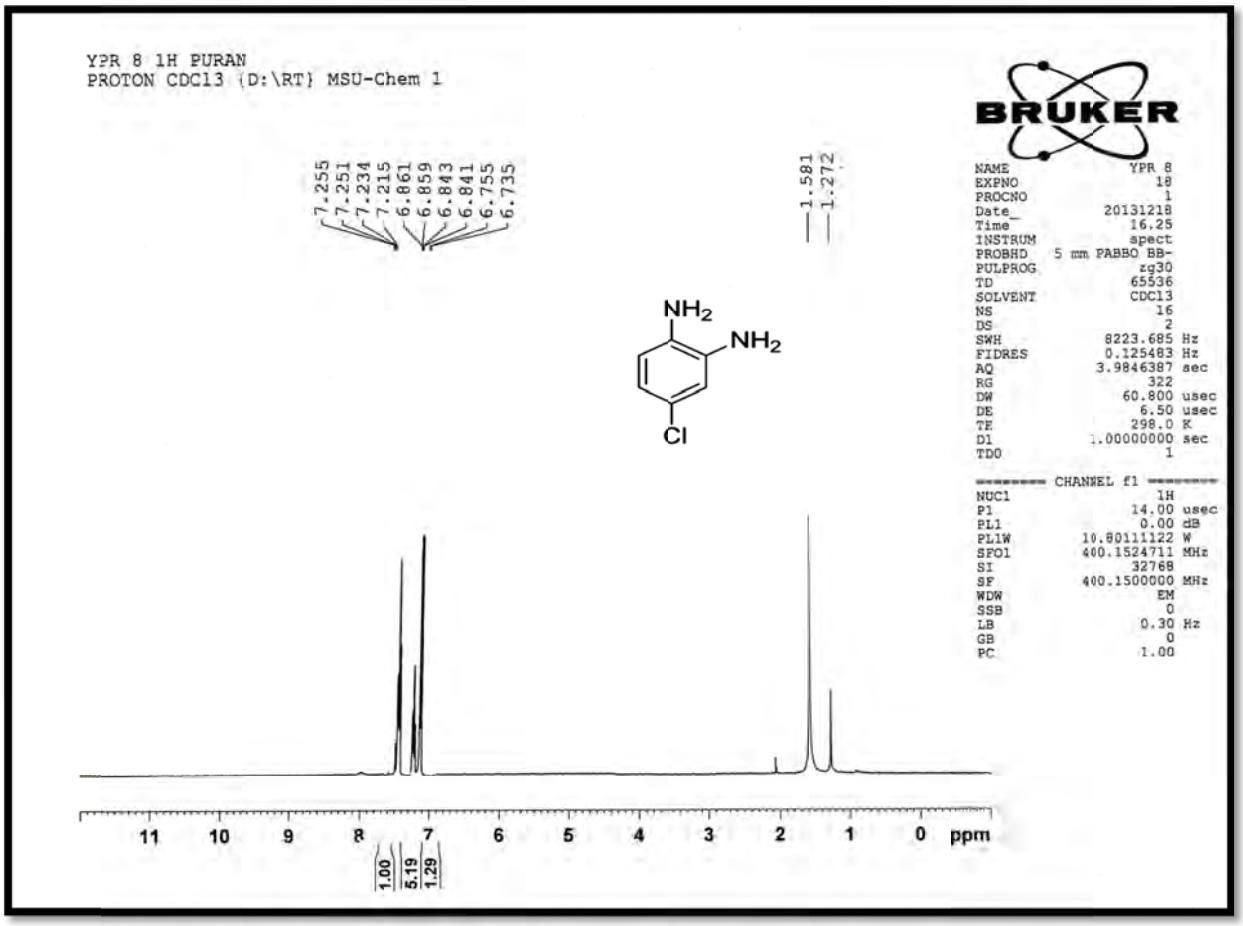

Fig. S20 ^{1}HNMR spectra of 4-Chlorobenzene-1, 2-diamine ($CDCl_3$, Table-2, Entry-11)

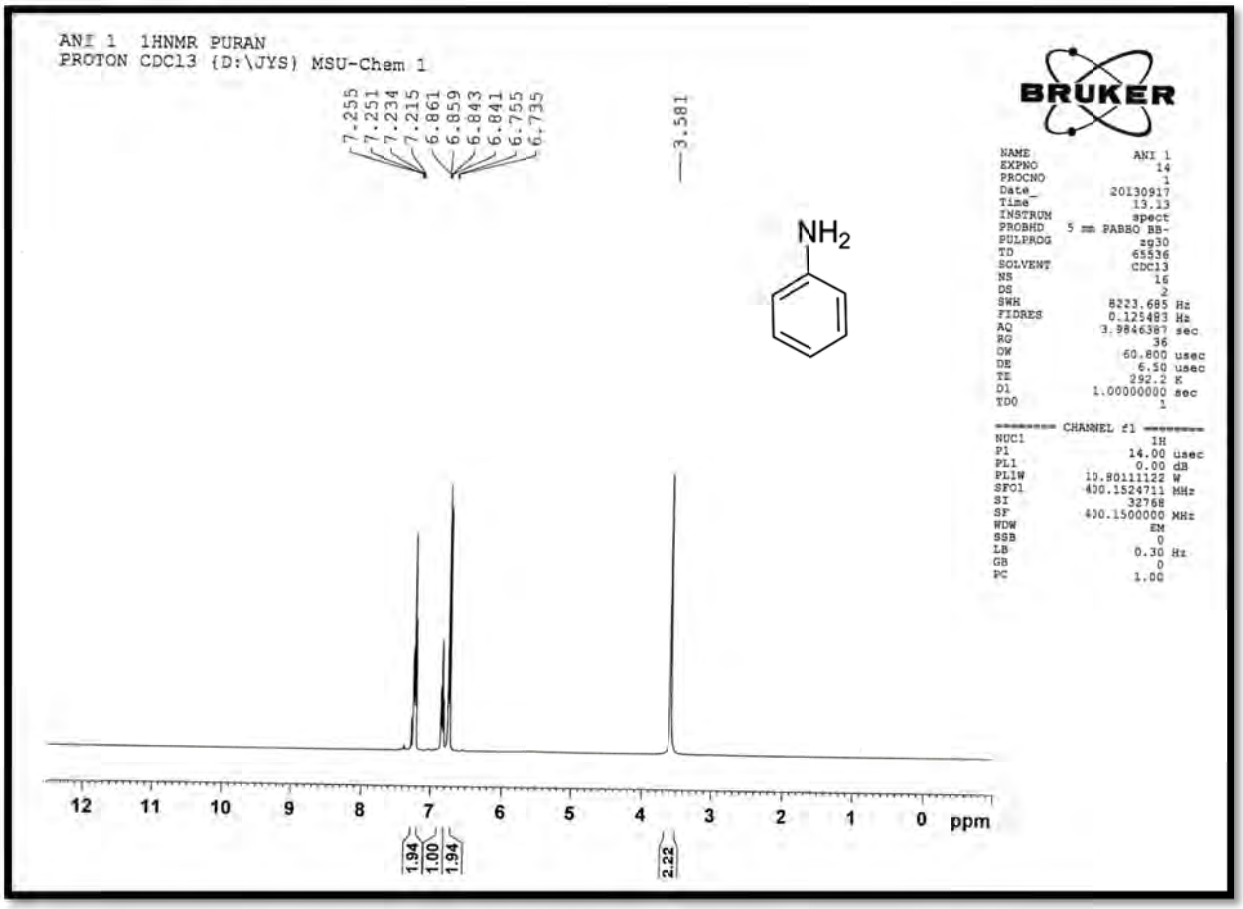

Fig. S21 ^{1}HNMR spectra of Aniline ($CDCl_3$, Table-2, Entry-12)

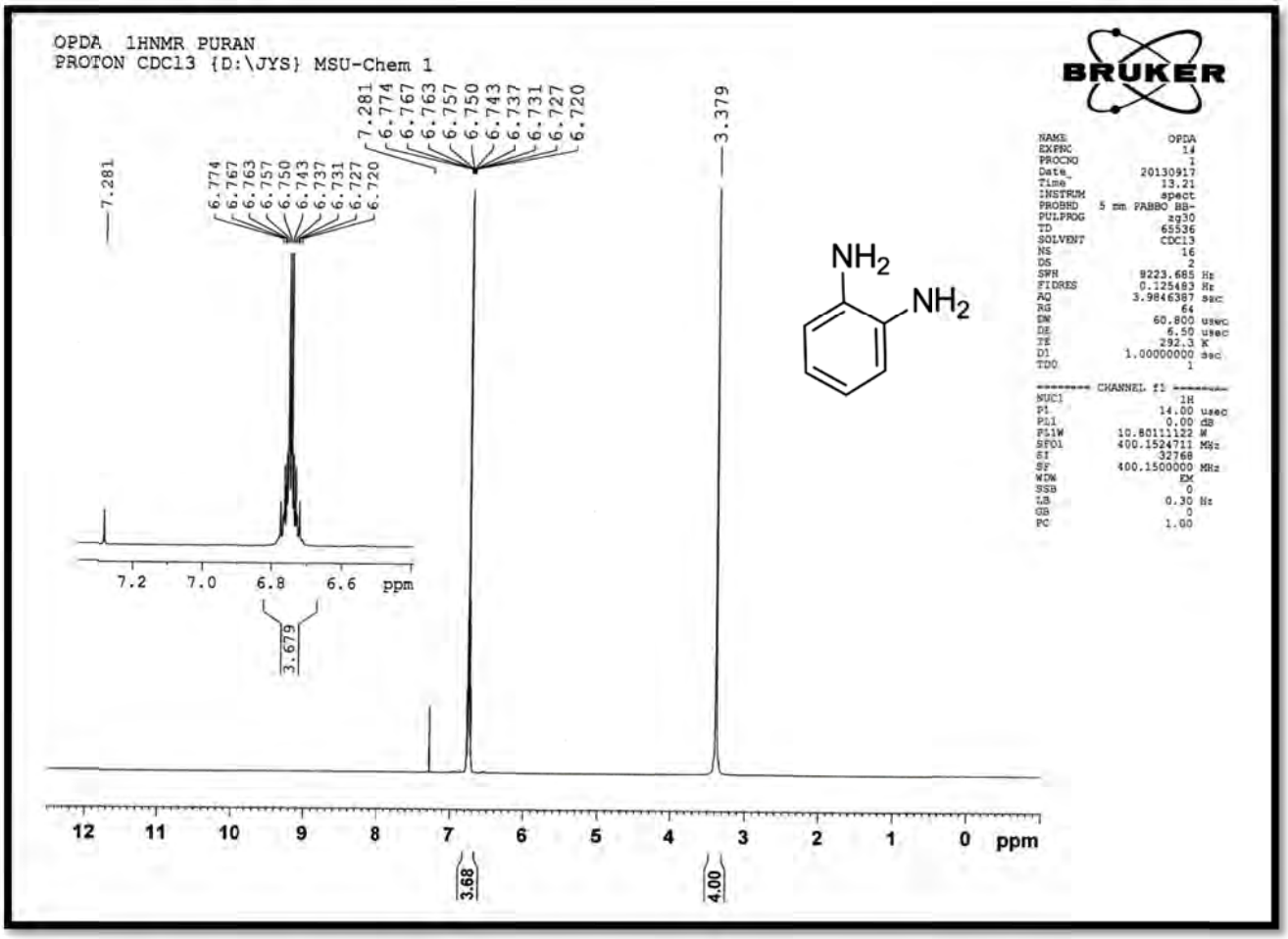

Fig. S22 ^{1}HNMR spectra of *o*-Phenylenediamine ($CDCl_3$, Table-2, Entry-13 and similar spectra for Entry-26)

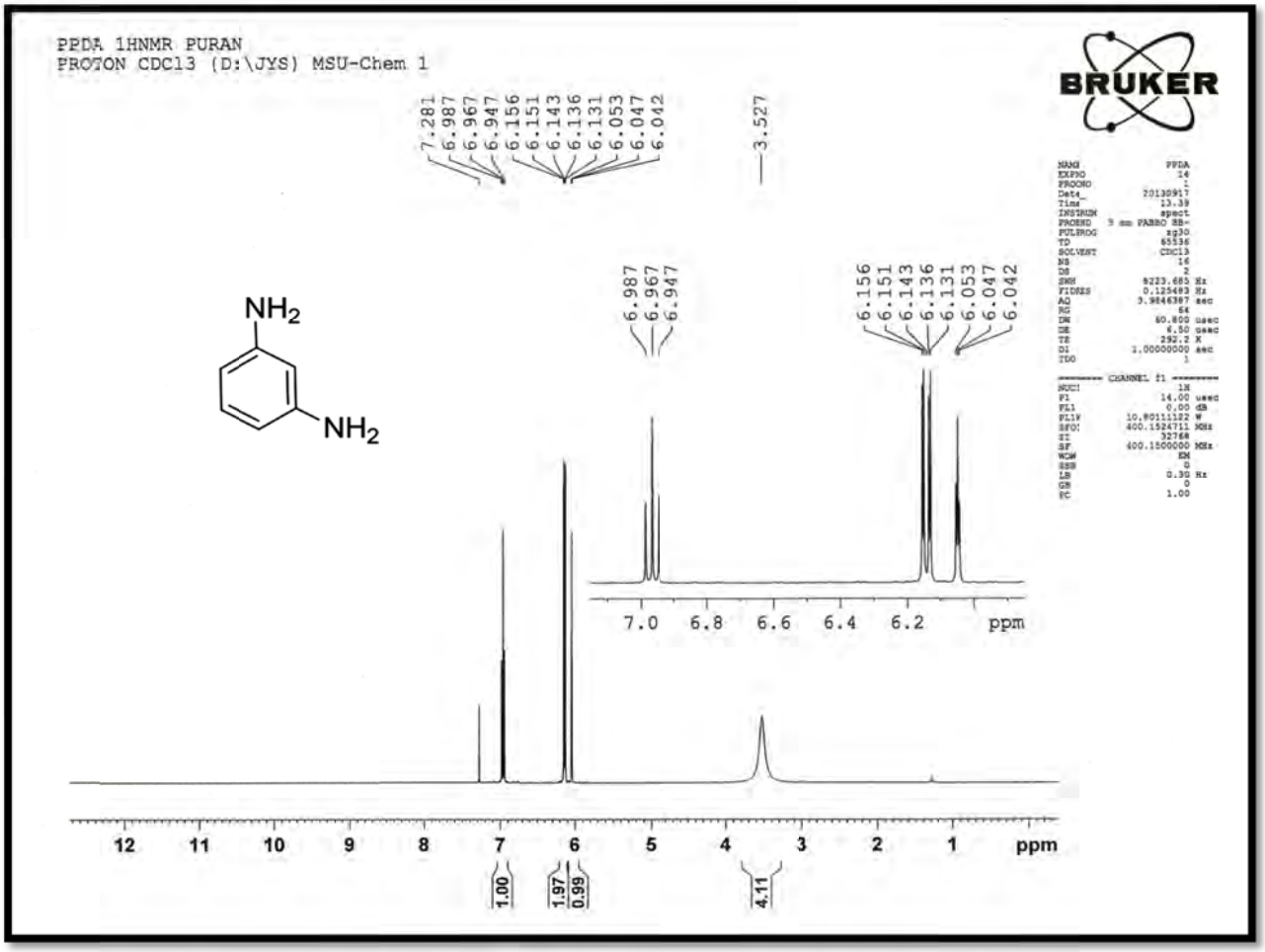

Fig. S23 ^{1}HNMR spectra of *m*-Phenylenediamine ($CDCl_3$, Table-2, Entry-14 and similar spectra for entry-25)

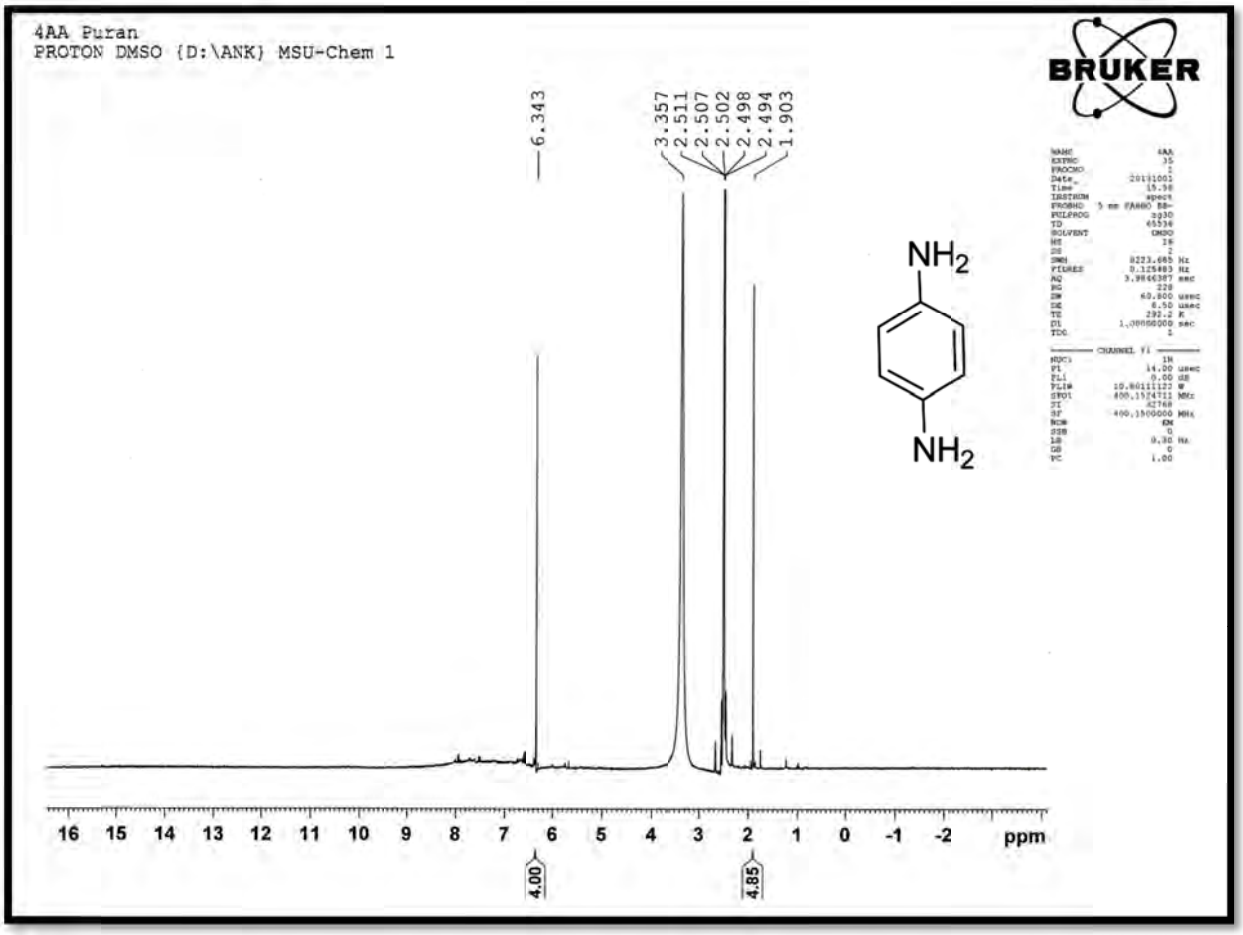

Fig. S24 ^{1}HNMR spectra of *p*-Phenylenediamine (DMSO, Table-2, Entry-15 and similar spectra for entry-27)

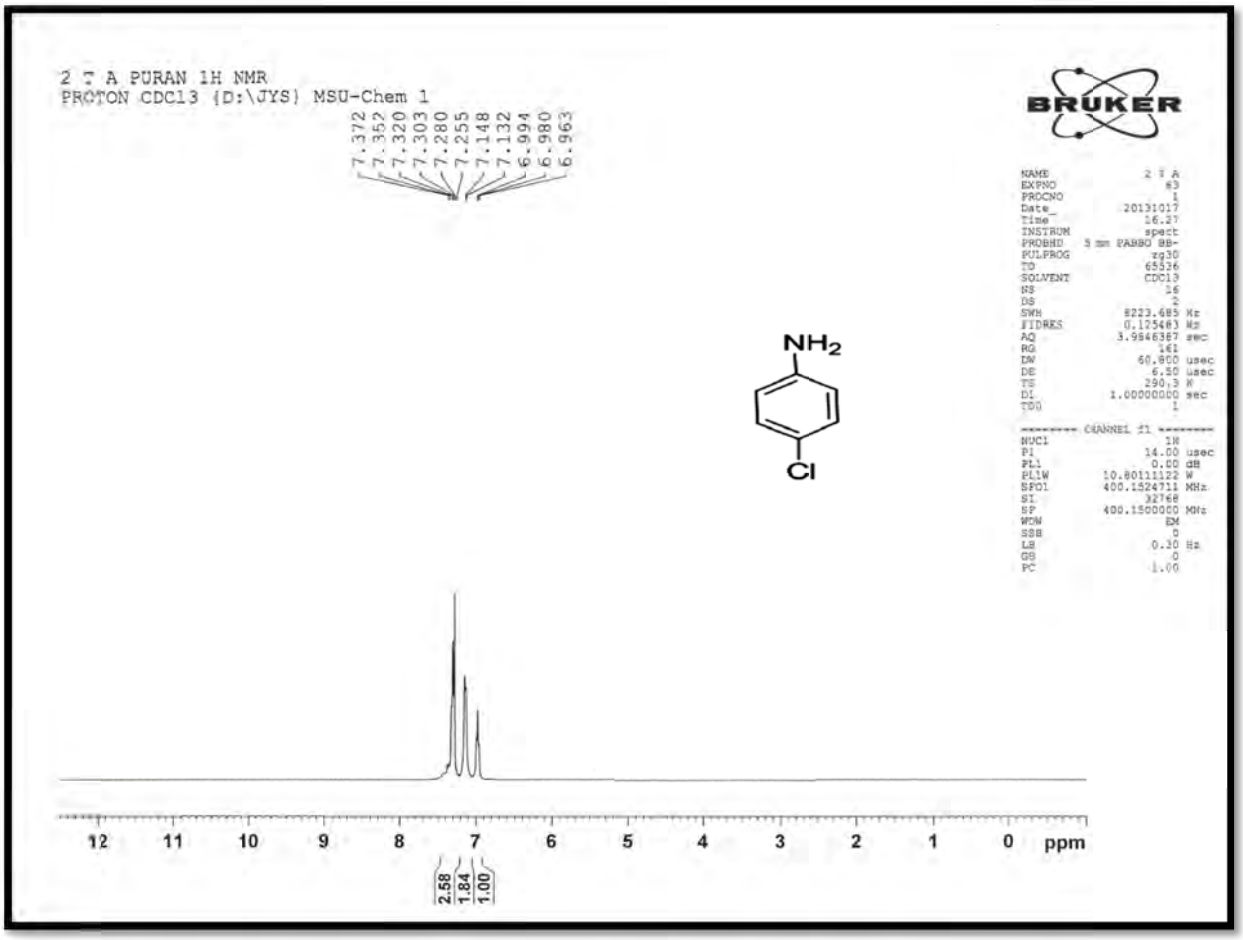

Fig. S25 ^{1}HNMR spectra of *p*-Chloroaniline ($CDCl_3$, Table-2, Entry-16)

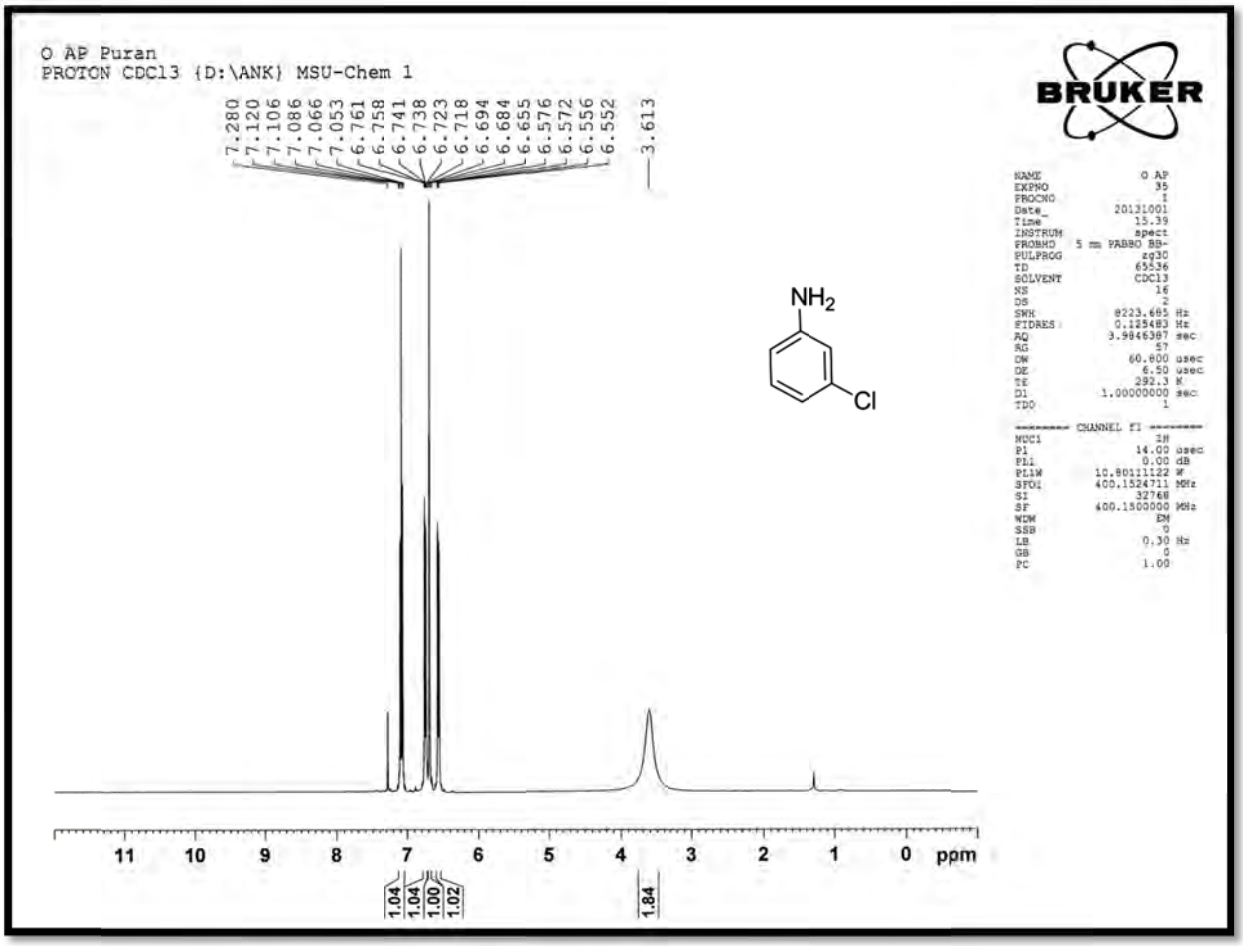

Fig. S26 ^{1}HNMR spectra of *m*-Chloroaniline ($CDCl_3$, Table-2, Entry-17)

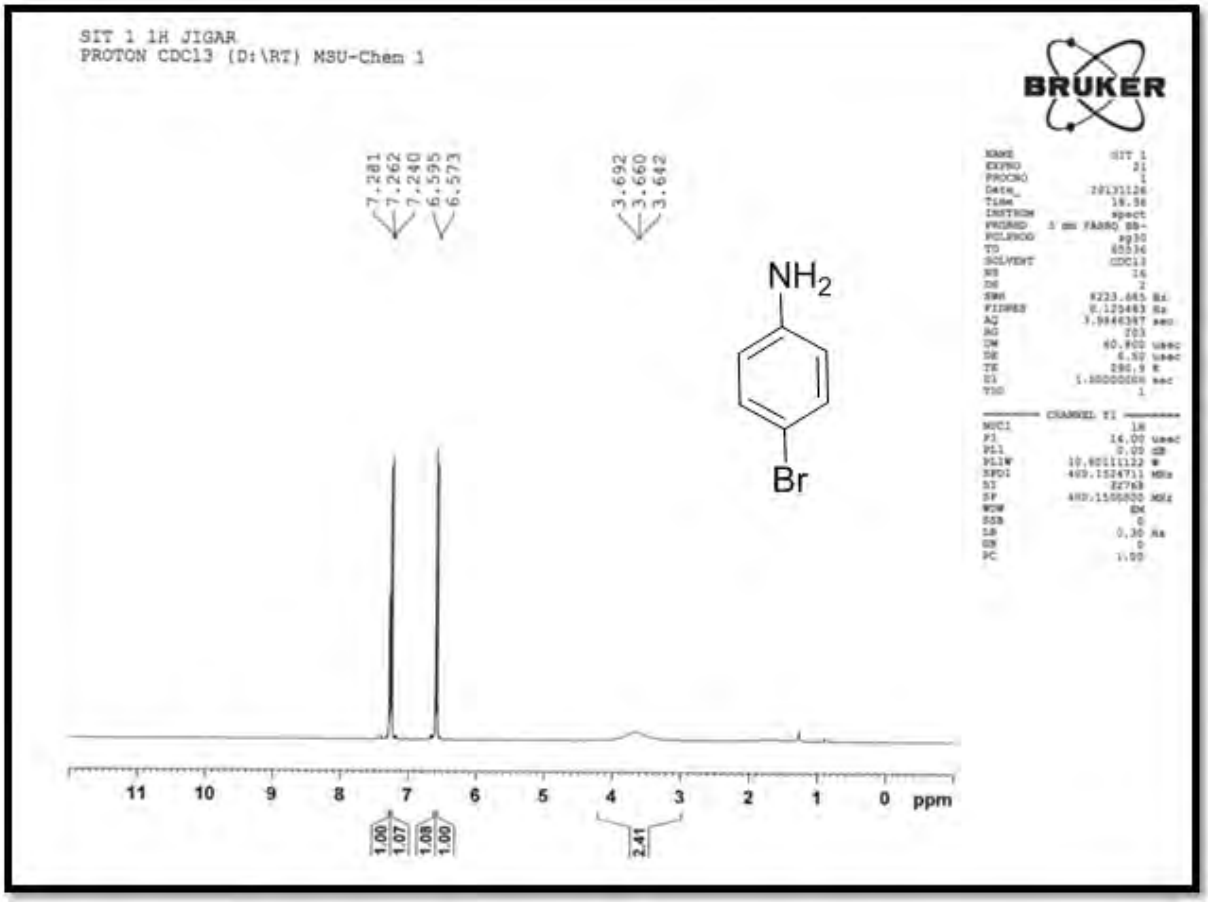

Fig. S27 ^{1}HNMR spectra of *p*-Bromoaniline ($CDCl_3$, Table-2, Entry-18)

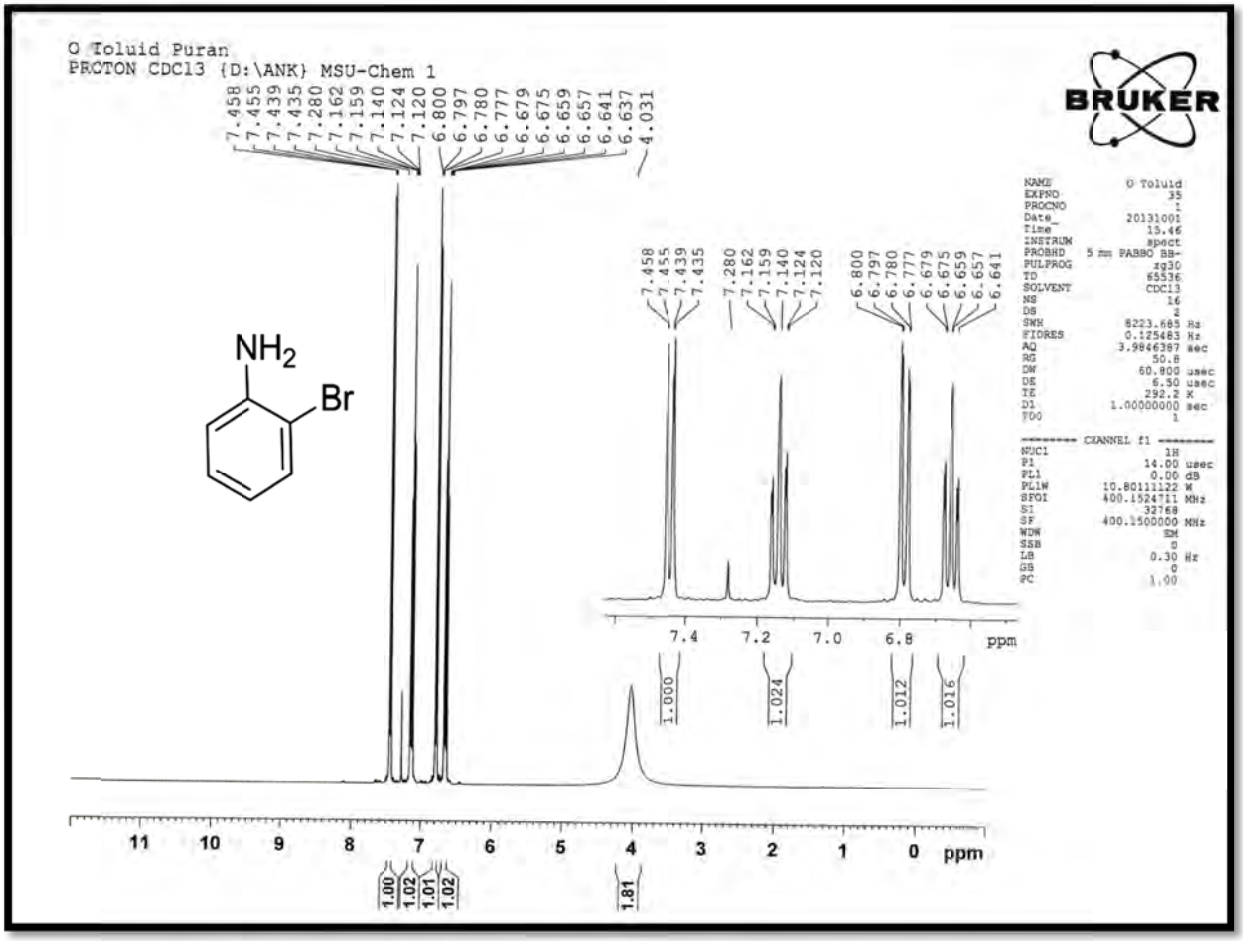

Fig. S28 ^{1}HNMR spectra of *o*-Bromoaniline ($CDCl_3$, Table-2, Entry-19)

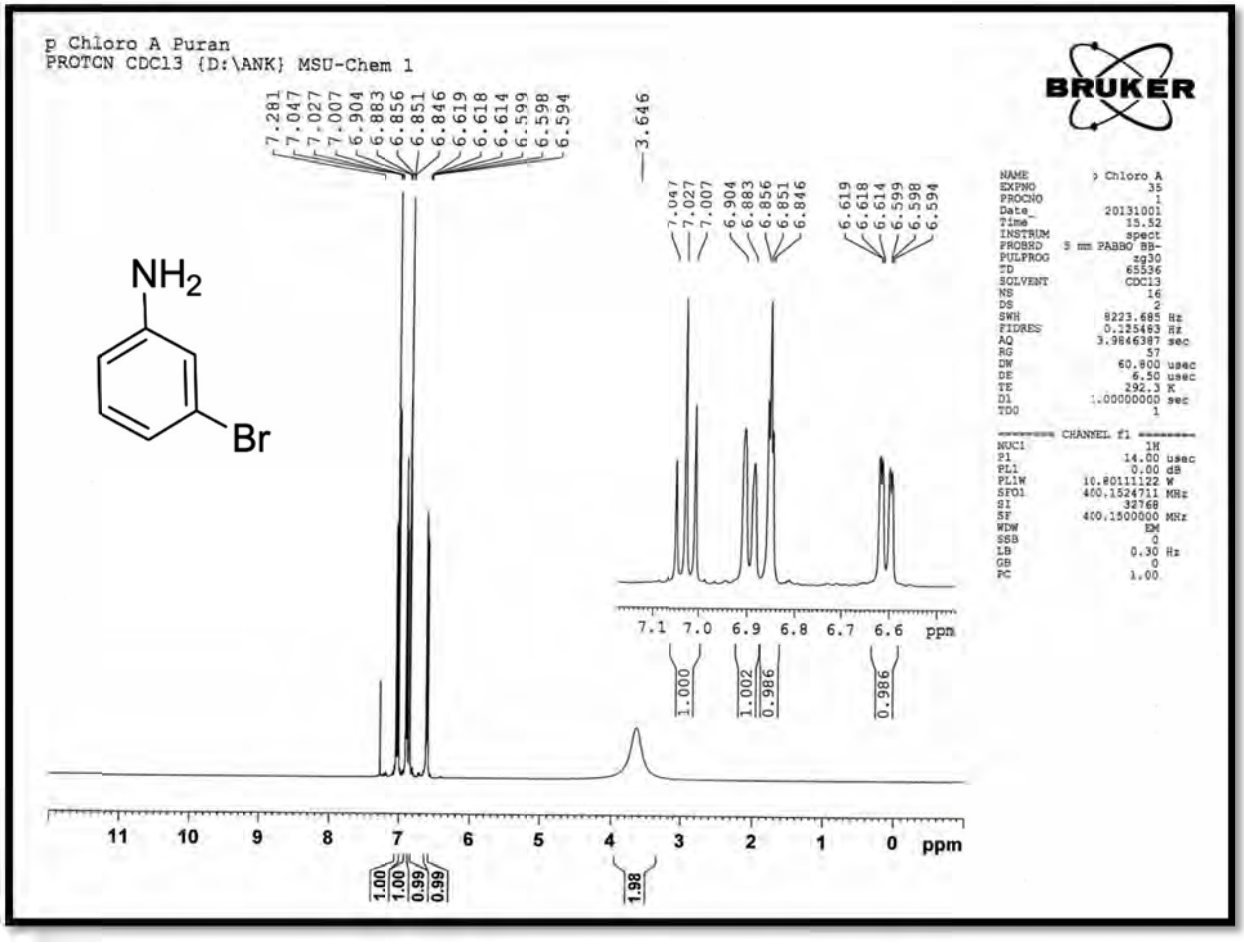

Fig. S29 ^{1}HNMR spectra of *m*-Bromoaniline ($CDCl_3$, Table-2, Entry-20)

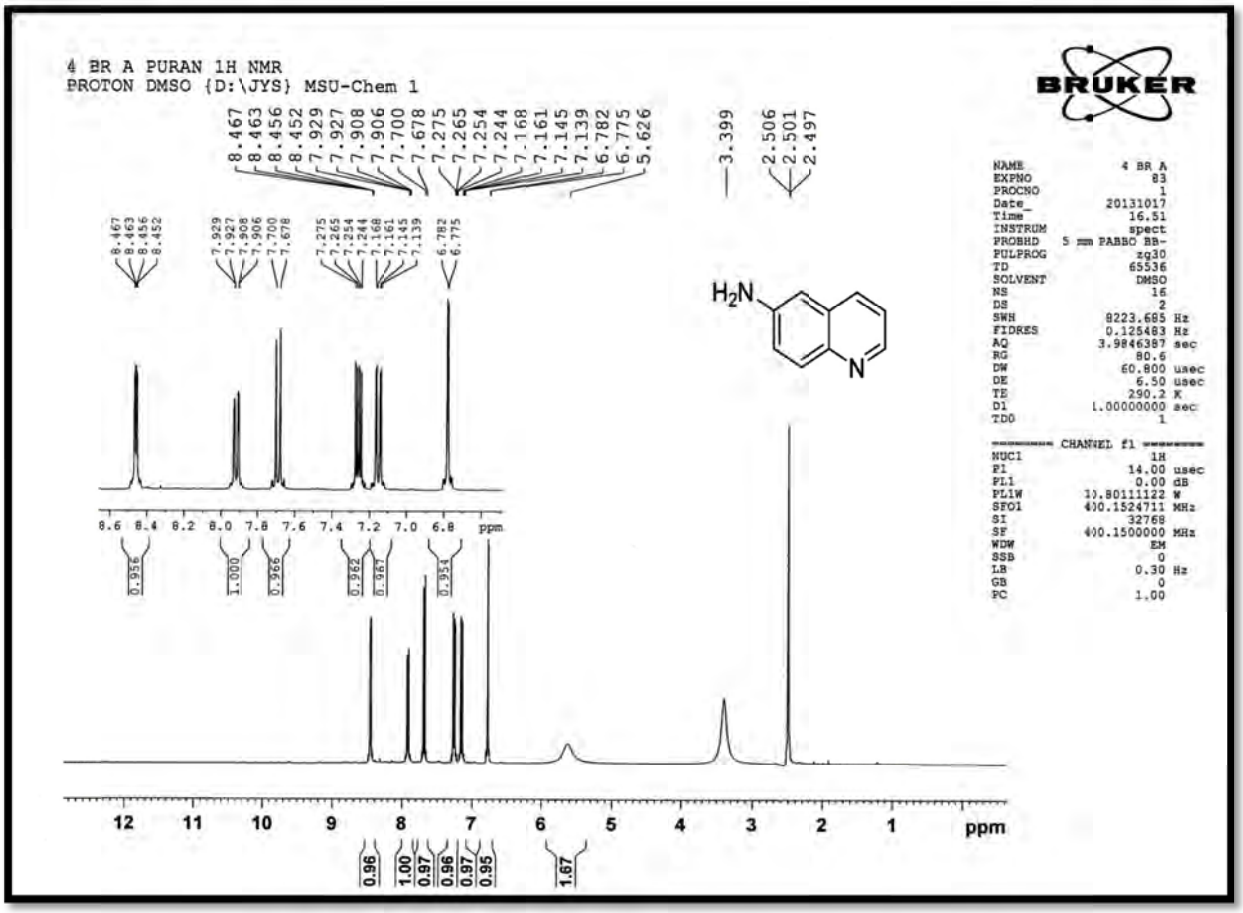

Fig. S30 ^{1}HNMR spectra of Quinolin-6-amine (DMSO, Table-2, Entry-21)

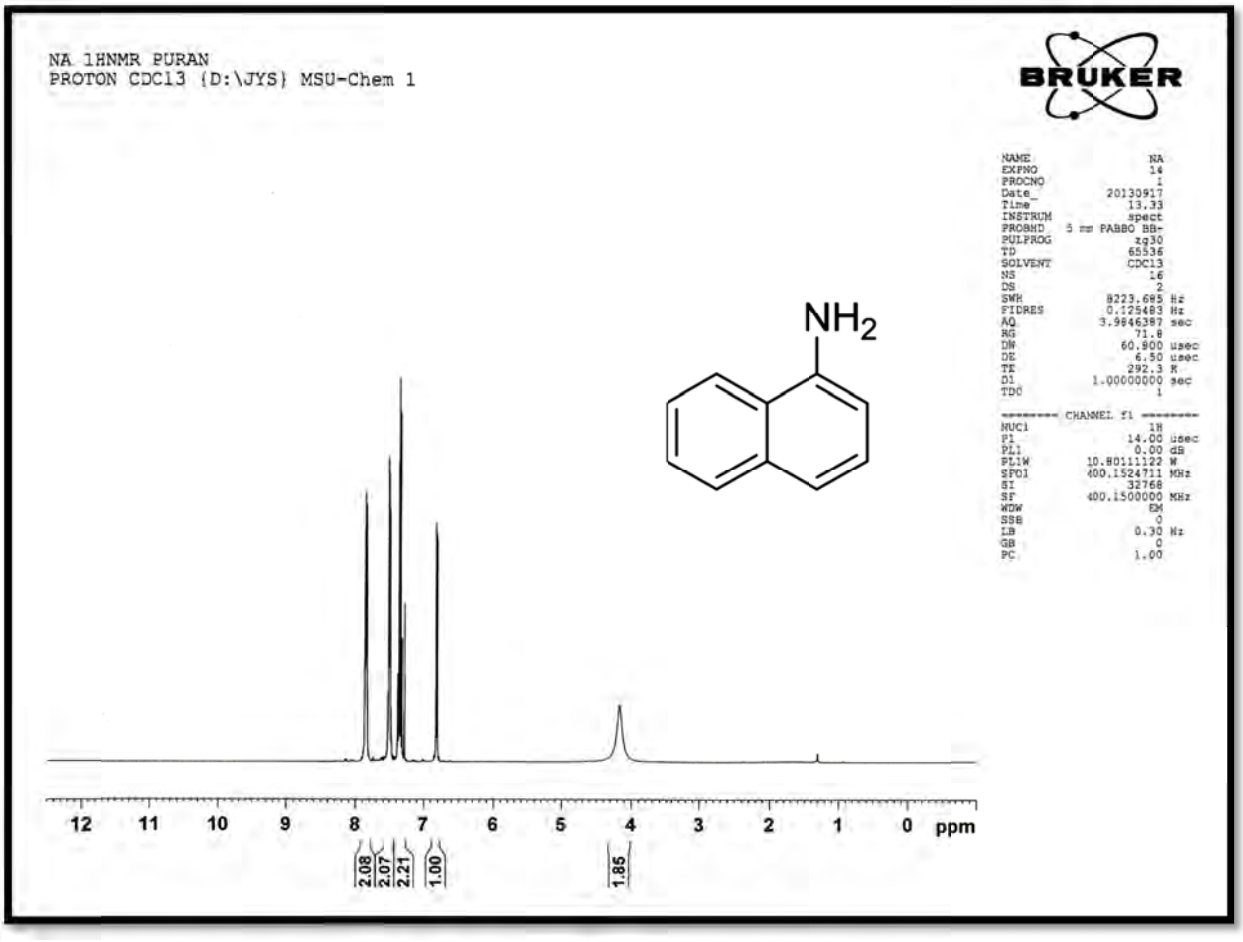

Fig. S31 ^{1}HNMR spectra of 1-Naphthylamine ($CDCl_3$, Table-2, Entry-22)

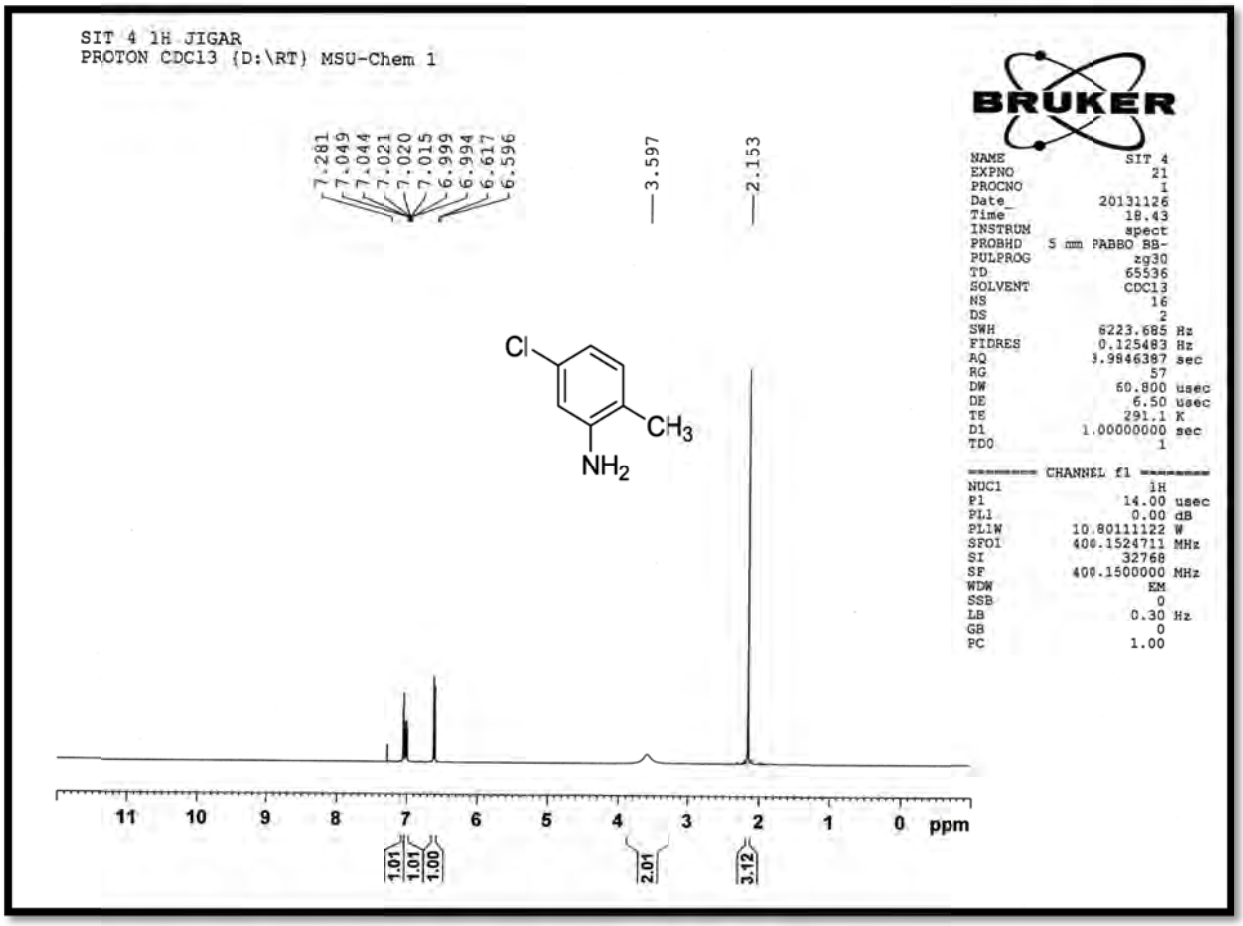

Fig. S32 ^{1}HNMR spectra of 2-Amino-5-Chlorotoluene ($CDCl_3$, Table-2, Entry-23)

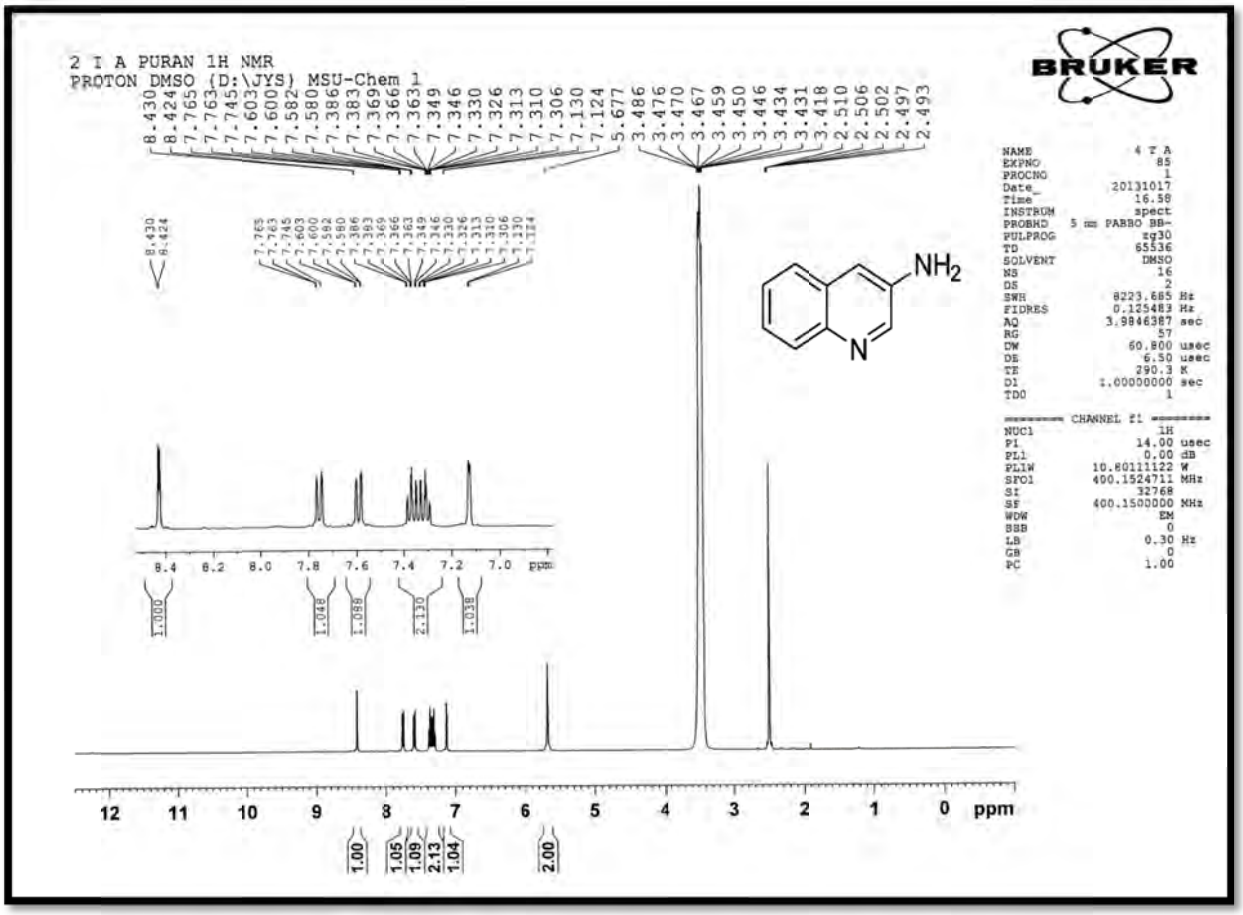

Fig. S33 ^{1}HNMR spectra of Quinolin-3-amine (DMSO, Table-2, Entry-24)

Table- 1 to 4 Shows XRD peak analysis of iron oxides

Phase – I

Pattern number: COD9006316, System: Cubic

Formula: $Fe_{2.667}O_4$ **Maghemite (γ-Fe_2O_3)**

Table-1

2θ (degrees)	(hkl)
30.30	202
35.632	311
43.341	400
53.877	422
57.346	333
63.00	404

Phase – II

Pattern number: COD1011032 System: FCC (Cubic)

Formula: Fe_3O_4 **Magnetite (Fe_3O_4)**

Table-2

2θ (degrees)	(hkl)
18.418	111
30.300	202
35.696	131
37.431	222
43.406	040
53.877	242
57.539	151
63.128	404

Phase – III

Pattern number: COD5910082 System: Hexagonal

Formula: Fe_2O_3 **Hematite (α-Fe_2O_3)**

Table-3

2θ (degrees)	(hkl)
24.261	0,1,2
33.319	0,-1,4
35.825	-1,-1,0
49.766	0,2,4
54.391	1,1,6
62.807	2,1,4
64.349	3,0,0

Phase – IV

Pattern number: COD1009073 System: Orthorhombic

Formula: FeOOH **Goethite**

Table-4

2θ (degrees)	(hkl)
27.024	110
36.146	011
36.339	200

Table-5 Leaching study by AAS after each recycling experiment[a]

Cycle	Fe leaching (ppm)	Ni leaching (ppm)	Cycle	Fe leaching (ppm)	Ni leaching (ppm)	Cycle	Fe leaching (ppm)	Ni leaching (ppm)
1	0.067	0.028	11	0.052	0.034	21	0.022	0.020
2	0.026	0.036	12	0.089	0.058	22	0.012	0.023
3	0.105	0.020	13	0.045	0.045	23	0.078	0.024
4	0.102	0.021	14	0.100	0.045	24	0.012	0.025
5	0.052	0.025	15	0.101	0.025	25	0.015	0.025
6	0.022	0.028	16	0.023	0.052	26	0.010	0.012
7	0.101	0.025	17	0.028	0.012	27	0.045	0.023
8	0.082	0.024	18	0.014	0.010	28	0.013	0.029
9	0.025	0.023	19	0.045	0.019	29	0.014	0.022
10	0.007	0.024	20	0.111	0.018	30	0.012	0.021

a- All experiment were carried out under optimum condition